DOI: 10.1002/chem.200802035

Regioselectivity Control in the Metal-Catalyzed Functionalization of γ-Allenols, Part 2: Theoretical Study[#]

Benito Alcaide,*[a] Pedro Almendros,*[b] Teresa Martínez del Campo,[a] Elena Soriano,*[b] and José L. Marco-Contelles[b]

Dedicated to Professor Franco Fernández on the occasion of his 65th birthday

Abstract: The gold-, palladium- and lanthanum-catalyzed oxycyclization reactions of azetidin-2-one-tethered γ-allenol derivatives to a variety of fused enantiopure tetrahydrofurans, dihydropyrans, and tetrahydrooxepines have been developed experimentally (Part 1, accompanying paper). The mechanisms of these regiocontrolled metal-catalyzed heterocyclization reactions have now been computationally explored at the DFT level (Part 2). The energies of the reaction intermediates and transition states for different possible pathways have been calculated in various model systems very close to the real system. Additionally, we selected the $La[N(SiH_3)_2]_3$ complex to simulate the lanthanide amide precatalyst species. The agreement of theoretically predicted and experimentally observed selectivities is very good in all cases

Keywords: allenes · cyclization · density functional calculations · gold · palladium

Introduction

Transition-metal-catalyzed cyclizations of allenes provide rapid routes to certain molecular skeletons, although the efficiencies of these reactions can be limited by regioselectivity issues.[1] It is well known in the chemistry of allenes that the regioselectivities of the reactions mainly depend upon the metal catalysts employed. In most cases, the substrate structure, not the reagent, is the controlling factor in the selective reaction of one double bond of the allene over the other. In this context, transition metal-catalyzed-cyclization of functionalized allenes bearing nucleophilic centers, such as allenols, has become a useful methodology for the synthesis of heterocycles.[2] In the preceding contribution (Part 1, accompanying paper),[3] we describe versatile regiocontrolled metal-catalyzed heterocyclization reactions of azetidin-2-one-tethered γ-allenol derivatives leading to a variety of fused enantiopure tetrahydrofurans, dihydropyrans, and tetrahydrooxepines. Regioselectivity control in the O–C functionalization of γ-allenols can be achieved through the choice of catalyst: $AuCl_3$ exclusively affords tetrahydrofurans, $La[N(SiMe_3)_2]_3$ usually favors the formation of dihydropyrans, whereas $PdCl_2$ entirely gives tetrahydrooxepines. In addition, it has been observed that for the Au-catalyzed cycloisomerization, a methoxymethyl protecting group not only masks a hydroxy functionality, but also exerts directing effects as a controlling unit in a regioselectivity reversal (7-*endo* versus 5-*exo* cyclization). In addition, the regioselectivity of the La-catalyzed cycloetherification can be tuned (5-*exo* versus 7-*endo*) simply through a subtle variation in the substitution pattern of the allene component (Ph versus Me). Thus, for the first time the regiocontrolled heterocyclization of γ-allenol derivatives is both catalyst- and substrate-directable.

[a] Prof. Dr. B. Alcaide, T. Martínez del Campo
Departamento de Química Orgánica I
Facultad de Química
Universidad Complutense de Madrid
28040 Madrid (Spain)
Fax: (+34) 91-3944103
E-mail: alcaideb@quim.ucm.es

[b] Dr. P. Almendros, Dr. E. Soriano, Prof. Dr. J. L. Marco-Contelles
Instituto de Química Orgánica General
Consejo Superior de Investigaciones Científicas, CSIC
Juan de la Cierva 3, 28006 Madrid (Spain)
Fax: (+34) 91-5644853
E-mail: Palmendros@iqog.csic.es
esoriano@iqog.csic.es

[#] For Part 1, see ref. [3].

Supporting information for this article is available on the WWW under http://dx.doi.org/10.1002/chem.200802035.

The lack of mechanistic information on allenol heterocyclization reactions prompted us to investigate the mechanistic course of the above processes at a theoretical level. Here we report the results of a computational study of the regiocontrolled metal-catalyzed cycloetherification reactions of azetidin-2-one-tethered γ-allenols.

Computational Methods

The density functional theory (DFT) calculations were performed with the aid of the Gaussian 03 package.[5] The B3LYP hybrid functional of Becke and of Lee, Yang, and Parr was used.[6] The 6-31 G(d) basis set was used for main-group atoms, while the metal centers Au, Pd, and La were described with the LANL2DZ basis set,[7] in which the innermost electrons are replaced by a relativistic effective core potential (ECP) and the valence electrons are explicitly treated by a double-ζ basis set. The optimized geometries were characterized by harmonic analysis, and the natures of the stationary points were determined according to the number of negative eigenvalues of the Hessian matrix. The intrinsic reaction coordinate (IRC) pathways from the transition structures were followed with a second-order integration method to verify the connections with the correct local minima.[8] The reported energies, enthalpies, and free-energies include the vibrational gas-phase zero-point energy term and thermal corrections, respectively. Solvent effects were allowed for through single-point calculations on the gas-phase optimized geometries. The conductor polarizable continuum model (CPCM)[9] as implemented in the Gaussian 03 package was used, with the parameters chosen by default. CH_2Cl_2, DMF, and toluene were selected as model solvents, with dielectric constants $\varepsilon = 8.93$, 39.0, and 2.38, respectively. Natural bond orbital (NBO) analyses[10] were performed with the module NBO v.3.1 implemented in Gaussian 03 to evaluate the NPA charges at the optimization level. To overcome an inherent error in the NBO module as implemented in Gaussian 03 for the La complexes,[11] the LANL2DZ basis set was applied augmented by addition of an f orbital.

Results and Discussion

To obtain insights into the factors that govern the regioselectivities of the transition-metal-catalyzed cyclizations and the roles of substituents, we performed a theoretical study on different precursors. Taking account both of the experimental observations (Part 1, accompanying paper) and of the available computational resources, we selected precursors **I**–**III** (see below) as theoretical models for the gold- and palladium-catalyzed reactions. In order to elucidate general mechanistic aspects of the intramolecular lanthanide-catalyzed hydroalkoxylation/cyclization of γ-allenols **4**, to

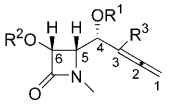

I: R^1 = TMS; R^2 = H; R^3 = Me
II: R^1 = MOM; R^2 = H; R^3 = Me
III: R^1 = COPh; R^2 = MOM; R^3 = Me
IV: R^1 = MOM; R^2 = H; R^3 = Ph

determine factors that govern the observed high regio- and stereoselectivities, as well as to highlight the roles of substituents, we have performed a computational study on the hydroalkoxylation of precursors **I**, **II**, and **IV** (see above) as theoretical models. Additionally, we also selected the La[N-$(SiH_3)_2$]$_3$ complex to simulate the precatalyst species.

The experimental results shown in Table 3 and Scheme 2 in Part 1 (accompanying paper)[3] suggest different activation modes of the allene moiety on complexation with the different catalysts. Unfortunately, the computed NPA charges on the reactant complexes **I**·$AuCl_3$ and **I**·$PdCl_2$ reveal similar trends. Complexation on the proximal allenic double bond (mode **a**, Figure 1) induces a stronger electrophilic

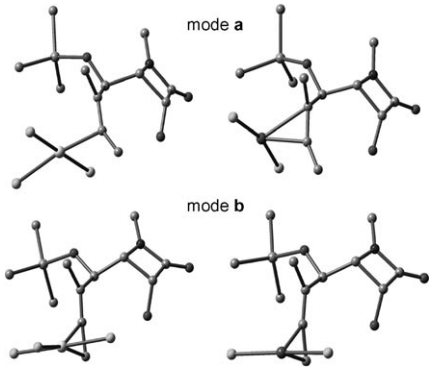

Figure 1. Optimized structures of the reactant complexes. Mode **a** relates to coordination of the proximal allene C=C, and mode **b** to coordination of the distal C=C. Hydrogen atoms have been omitted for clarity.

character at C3 (Table 1; see also Figure 2 for orbital topology), hence preferentially promoting a 5-*exo-trig* cyclization. Because of the hindrance between the catalyst and the TMS group, the allene moiety coordinates the metal center only through C2 (Au–C2 = 2.211 Å), forming a slipped η^1-reactant complex, **I**·$AuCl_3$, whereas the less sterically demanding $PdCl_2$ forms a η^2-complex through coordination of C2 and C3 (2.057 and 2.279 Å, respectively). The engagement of the distal allenic double bond (mode **b**, Figure 1) enhances the electrophilic character at the central allene carbon C2 (Table 1). The lower steric hindrance induced by the methyl substituent allows the formation of a more symmetric complex with the gold catalyst (Au–C1 2.283, Au–C2 2.489 Å). In the case of the complex formed by π-coordination of the

Abstract in Spanish: *La reacción de heterociclación de γ-alenoles catalizada por metales es un proceso regiocontrolado que da lugar a una amplia variedad de tetrahidrofuranos, tetrahidropiranos y tetrahidrooxepinas fusionadas enantiopuras, que contienen además un anillo β-lactámico, que es la unidad estructural clave en productos biológicos relevantes como antibióticos e inhibidores enzimáticos. Se ha llevado a cabo un estudio teórico para la elucidación de los mecanismos de estas ciclaciones catalizadas por oro, paladio y lantano, en estrecha relación con el trabajo experimental (Parte 1, artículo anterior), corroborando los resultados obtenidos en el laboratorio.*

Table 1. NPA atomic charges on the reactant complexes. The charge for the uncomplexed precursor is also shown, to illustrate the effect of the catalyst.[a]

Mode[a]		C1	C2	C3	C4	C5	C6	O	M	MCl_n
–	–	−0.495	+0.072	−0.122	+0.091	−0.073	+0.026	−0.738	–	–
a	$AuCl_3$	−0.386	−0.188	+0.158	+0.065	−0.075	+0.027	−0.740	+0.996	−0.319
a	$PdCl_2$	−0.418	−0.012	+0.050	+0.083	−0.076	+0.028	−0.738	+0.716	−0.339
b	$AuCl_3$	−0.473	+0.133	−0.065	+0.108	−0.066	+0.029	−0.764	+1.011	−0.297
b	$PdCl_2$	−0.428	+0.057	−0.065	+0.104	−0.064	+0.029	−0.763	+0.719	−0.289

[a] Mode **a**: coordination of the proximal allene C=C. Mode **b**: coordination of the distal C=C.

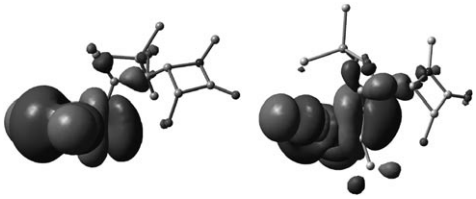

Figure 2. Topologies of the acceptor molecular orbital LUMOs on the complexed structure precursors of **I** according to the mode of coordination: mode **a** (left) and mode **b** (right).

proximal allenic double bond, the net charge transfer from the π system to the catalyst is slightly larger than that computed from the distal bond (MCl_n, Table 1), which produces a more electrophilic allene moiety (mainly at C3).

On the basis of these electronic data, these binding modes would preferably promote either 5-*exo-trig* or 6-*exo-dig* cyclization through intramolecular nucleophilic addition by alternative paths, to form tetrahydrofuran or dihydropyran skeletons, respectively. However, the fact that divergent results are observed suggests that other factors must also come into play. Firstly, we focused on the $AuCl_3$-catalyzed cycloisomerization of **I**. The computed energy values clearly reveal a kinetic preference for the formation of the fused tetrahydrofuran scaffold (Table 2). The free energy barrier to reach the transition structure $\mathbf{TS_{I\text{-}5}}$ is thus 5.1 and 8.2 kcal mol^{-1} lower than the corresponding transition structures for addition to the central ($\mathbf{TS_{I\text{-}6}}$) and the terminal allene carbon ($\mathbf{TS_{I\text{-}7}}$), respectively (Figure 3). These results agree with experimental evidence.

From a thermodynamic viewpoint, the formation of the tetrahydrooxepine intermediate ($\mathbf{IN_{I\text{-}7}}$) is slightly more exothermic than the formation of the tetrahydrofuran ($\mathbf{IN_{I\text{-}5}}$) and dihydropyran ($\mathbf{IN_{I\text{-}6}}$) intermediates. In this regard, the most stable structure in the gas phase is the tetrahydrofuran complex, but solvent effects exert a larger effect on the stabilization of the seven-membered ring. The transition structures and subsequent intermediates show the formation of a weak hydrogen bond between one of the chloride ligands and the acidic hydroxy hydrogen (for $\mathbf{TS_{I\text{-}5}}$, $\mathbf{TS_{I\text{-}6}}$, $\mathbf{TS_{I\text{-}7}}$: 2.240, 3.793, 2.242 Å; for $\mathbf{IN_{I\text{-}5}}$, $\mathbf{IN_{I\text{-}6}}$, $\mathbf{IN_{I\text{-}7}}$: 1.790, 1.691, 1.875 Å). This interaction slightly stabilizes the structures relative to non-hydrogen-bonded structures (when this alternative is possible).

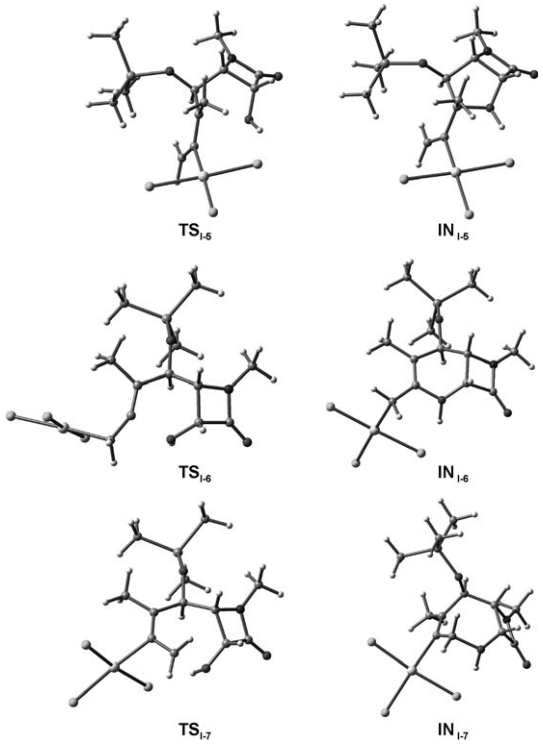

Figure 3. Optimized structures of the transition states and intermediates for the oxycyclization by alternative pathways.

Table 2. Enthalpy and free energy in the gas phase, as well as free energy in solution (kcal mol^{-1}) for the cyclization of **I** by alternative regioisomeric 5-*exo-trig*, 6-*exo-dig*, and 7-*endo-trig* pathways.

	$AuCl_3$			$PdCl_2$		
	ΔH_{gas}	ΔG_{gas}	ΔG_{sol}	ΔH_{gas}	ΔG_{gas}	ΔG_{sol}
$\mathbf{I}\cdot MCl_n$	0.0	0.0	0.0	0.0	0.0	0.0
$\mathbf{TS_{I\text{-}5}}$	3.7	6.1	1.9	6.2	7.5	4.8
$\mathbf{IN_{I\text{-}5}}$	−4.0	−2.7	−5.5	−2.8	−1.2	−2.3
$\mathbf{TS_{I\text{-}6}}$	8.3	9.6	7.0	15.2	15.9	9.5
$\mathbf{IN_{I\text{-}6}}$	−3.5	−2.6	−5.8	−2.1	−0.8	−1.9
$\mathbf{TS_{I\text{-}7}}$	14.2	15.0	10.1	15.9	17.9	11.2
$\mathbf{IN_{I\text{-}7}}$	−3.2	−2.5	−10.0	−1.5	0.1	−2.2

The fact that the cyclization generates a quaternary center in an asymmetric manner when a 5-*exo* cyclization route is followed is due to steric effects in the transition state. Thus, while

$\mathbf{TS_{I\text{-}5}}$ lacks unfavorable steric interactions, the formation of the epimer proceeds through the transition structure $\mathbf{TS_{I\text{-}5}'}$ (Figure 4), exhibiting distortion of the allenic group in order to alleviate the steric interaction with the protons at the lactam ring (distance from the terminal allenic proton to the lactam proton = 2.034 Å in $\mathbf{TS_{I\text{-}5}'}$, shorter than sum of van der Waals radii, versus the distance from the methyl proton to the lactam proton = 2.307 Å in $\mathbf{TS_{I\text{-}5}}$). This effect results in a transition structure 5.3 kcal mol^{-1} higher in energy than $\mathbf{TS_{I\text{-}5}}$, which accounts for the observed stereoselectivity.

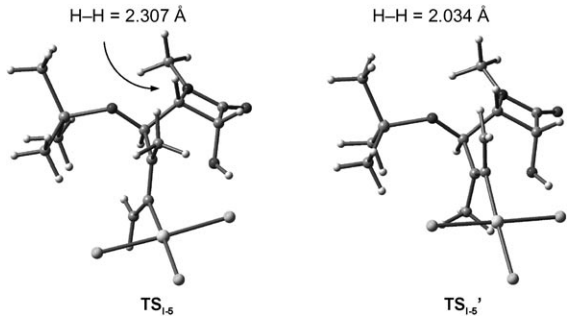

Figure 4. Transition structures for the 5-*exo-trig* cyclization, showing critical steric interactions that account for the observed stereochemistry.

The higher stability of the transition structure $\mathbf{TS_{I\text{-}5}}$, and hence the kinetic preference for the formation of the five-membered oxacycle, is mostly due to the electronic effects described above. In addition, steric hindrance produced by the TMS protecting group plays a significant role. As can be seen in Figure 3, the bulky TMS group on the tether center causes compression of the internal angle (C3-C4-C5 108.2°) to relieve the steric pressure with the allenic moiety and lactam ring, so the reactive centers at the ends of the system are moved closer together, thus favoring the cyclization and improving the reaction rate (Thorpe–Ingold effect). In contrast, the formation of the larger seven-membered ring proceeds through a transition structure $\mathbf{TS_{I\text{-}7}}$, in which the methyl substituent can rest in the same plane as the TMS group. This conformation is reached without angle compression; in fact, it proceeds with an angle opening (C3-C4-C5 119.7°) because the ring strain imposed by the lactam and endocyclic alkene group restrains the tether flexibility and the interaction between reactive centers. It should be noted, however, that a ring-puckering change upon optimization to the intermediate, $\mathbf{IN_{I\text{-}7}}$, is observed to relieve steric congestion in the cyclized adduct (Figure 3).

Protonolysis of the σ-carbon-gold bond would yield the bicycle type **5** with simultaneous regeneration of the Au^{III} species. This process could proceed through two conceivable paths from the vinyl-Au complex $\mathbf{IN_{I\text{-}5}}$: by a direct 1,3-H shift (pathway a), or through a stepwise migration assisted by the catalyst (pathway b) (Scheme 1).

The results, summarized in Table 3, clearly point to the stepwise mechanism as the most likely route. It should be noted that the first step is nearly thermoneutral and takes place with a negligible activation barrier (ΔG_{sol} = 0.3 kcal mol^{-1}) to afford an intermediate, $\mathbf{IN_{Hb}}$, that still exhibits a strong Au–Cl interaction (2.559 Å). This suggests that the ligand remains partially attached to the metal throughout the assisted H-shift. The last step could then be the cleavage of the Au–C bond by HCl, to liberate the bicycloadduct. The formation of the C–H bond and regeneration of the catalyst thus proceeds in a highly exothermic step through the transition structure $\mathbf{TS2_{Hb}}$, which involves a free energy barrier of 7.0 kcal mol^{-1}. The direct transformation (pathway a), via $\mathbf{TS_{Ha}}$, requires a significantly higher free energy of activation ($\Delta G_{\ddagger}^{sol}$ = 19.8 kcal mol^{-1}). The stepwise pathway is therefore predicted to be considerably fa-

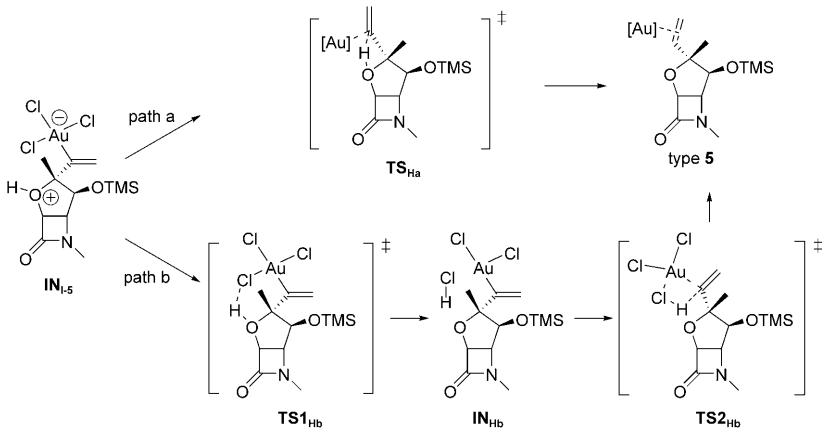

Scheme 1. Possible pathways for the production of the bicycle of type **5** through protonolysis.

Table 3. Free energy differences in solution (kcal mol^{-1}) for the 1,3-H shift from the 5-*exo* and 7-*endo* cyclized adducts.[a]

	$AuCl_3$		$PdCl_2$	
	$n=5$	$n=7$	$n=5$	$n=7$
$\mathbf{IN_{I\text{-}n}}$	0.0 (−5.5)	0.0 (−10.0)	0.0 (−2.3)	0.0 (−2.2)
$\mathbf{TS_{Ha}}$	19.8 (14.3)	19.2 (9.2)	20.8 (18.5)	21.3 (19.1)
$\mathbf{TS1_{Hb}}$	0.3 (−5.2)	0.4 (−9.6)	−0.1 (−2.4)	−0.4 (−2.6)
$\mathbf{IN_{Hb}}$	−0.3 (−5.8)	−0.9 (−10.6)	−0.2 (−2.5)	−0.5 (−2.7)
$\mathbf{TS2_{Hb}}$	6.7 (1.2)	8.6 (−2.4)	7.0 (4.7)	8.8 (6.6)
product	−22.3 (−27.8)	−19.6 (−29.6)	−19.7 (−22.0)	−16.0 (−18.2)

[a] Free energy differences relative to the reactant complex are shown in parenthesis.

vored (by 13.1 kcal mol^{-1}) over the concerted path, which can hence be ruled out as operative. Overall, the 1,3-H shift is a strongly exothermic process (−22.3 kcal mol^{-1}), pointing to a poorly reversible character.

To sum up, the Au^{III}-catalyzed cyclization of γ-allenol **I** (Figure 5) takes place regio- and stereoselectively through a 5-*exo* hydroalkoxylation because of a kinetic preference governed by electronic and steric factors.

A possible pathway for the production of the bicyclic tetrahydrofuran of type **5** from γ-allenol **I** might thus initially involve the formation of a complex **I**·$AuCl_3$ through coordination of the gold trichloride to the proximal allenic double bond. Next, regioselective 5-*exo* oxyauration forms zwitterionic species $\mathbf{IN_{I\text{-}5}}$. Loss of HCl, followed by protonolysis of the carbon-gold bond of $\mathbf{IN_{Hb}}$, affords a product of type **5** and regenerates the gold catalyst (Scheme 2).

The Pd^{II}-catalyzed cyclizative couplings of γ-allenols **4** with allyl halides gave the tetrahydrooxepine-β-lactams **7**

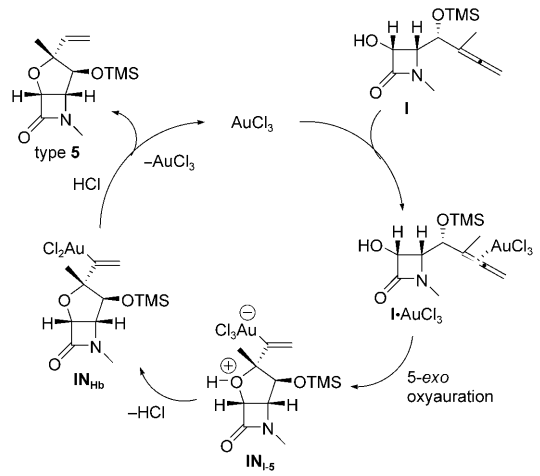

Scheme 2. Mechanistic explanation for the Au^{III}-catalyzed heterocyclization of γ-allenol **I**.

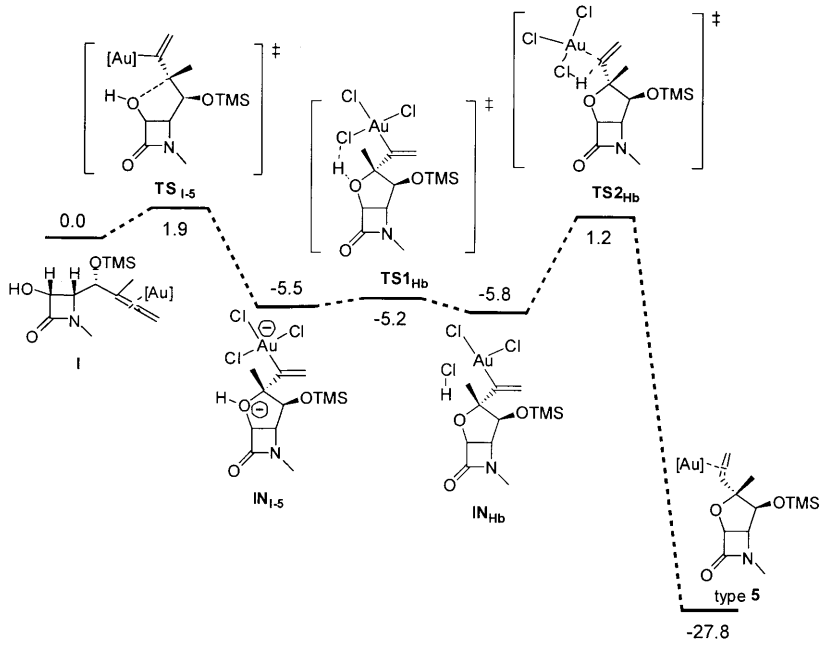

Figure 5. Free energy profile (kcal mol^{-1}) for the transformation of γ-allenol **I** into the tetrahydrofuran of type **5**.

(Scheme 2 in Part 1, accompanying paper), resulting from 7-*endo* oxycyclization. However, the computed results for the plausible cyclization modes on the allenol model **I** show the same trend as seen before for the Au^{III}-catalyzed process: namely, a kinetic preference for the 5-*exo-trig* cyclization, although the 7-*endo-trig* cyclization proceeds with a barrier only 6.4 kcal mol^{-1} higher (versus $\Delta G^{sol}_{\neq} = 8.2$ kcal mol^{-1} for Au^{III} catalysis). This weaker kinetic preference may be due to a lower polarization of the allene upon π-coordination to the metal (Table 1). In this context, we have explored every alternative process to determine the factors that promote the 7-*endo* over the 5-*exo* cyclization and the allyl coupling over the H-shift.

Whereas the transition structure for the 5-*exo-trig* cyclization appears to be slightly later for the Pd^{II}-catalyzed processes than for the Au^{III}-catalyzed ones (2.429 vs 2.457 Å, respectively), the alternative 7-*endo-trig* process is earlier (2.055 vs 1.942 Å, respectively). Likewise, the transition structures (very weak for $\mathbf{TS_{I\text{-}6}}$) and subsequent intermediates each show the formation of a hydrogen bond between the closest halide ligand and the hydroxy proton (for $\mathbf{TS_{I\text{-}5}}$, $\mathbf{TS_{I\text{-}6}}$, $\mathbf{TS_{I\text{-}7}}$: 2.177, 2.607, 2.145 Å; for $\mathbf{IN_{I\text{-}5}}$, $\mathbf{IN_{I\text{-}6}}$, $\mathbf{IN_{I\text{-}7}}$: 1.708, 1.707, 1.741 Å), which is stronger (shorter) than in the case of the related Au^{III}-complexed structures. This effect makes the first event of the 1,3-H shift (formation of $\mathbf{IN_{Hb}}$ intermediate, pathway b, Scheme 1) a barrierless step (Table 3). Although pallada-tetrahydrooxepine and pallada-furan intermediates show equivalent structural and energetic properties, we focus here on the former; discussion of the latter is presented below. The formed HCl shows a greater elongation of the Pd–Cl distance (hence, weaker interaction) in relation to the same state $\mathbf{IN_{I\text{-}7}}$ for the Au counterpart ($\Delta d_{M\text{–}Cl} = 0.10$ vs 0.06 Å, respectively; for optimized structures and selected geometric parameters for Au^{III} and Pd^{II}-mediated protonolysis of $\mathbf{IN_{I\text{-}7}}$ see the Supporting Information), which suggests easier HCl release. The final formation of the C–H bond and regeneration of the catalyst requires a low energy barrier of 8.3 kcal mol^{-1} to be overcome.

Alternatively, the presence of an allyl halide promotes a coupling reaction by trapping with the intermediate $\mathbf{IN_{Hb}}$. This process should be favored by the easy HCl release/metal decoordination. Furthermore, a close inspection of the vinyl intermediates $\mathbf{IN_{I\text{-}n}}$ suggests that this reaction should take place more favorably for the pallada-tetrahydrooxepine that for the pallada-furan intermediate because of lower steric hindrance around the reactive centers. The allyl coupling with the alkenyl Pd^{II} intermediate occurs through insertion into the allylic halide C=C bond to give a σ-C-Pd intermediate, which then undergoes a *trans* β-elimination to afford the oxepane product (Figure 6).[12] The weakly Pd-coordinated HCl in $\mathbf{IN_{Hb}}$ can be easily displaced by the incoming allyl bromide in a fast ligand-interchange displacement mechanism, which yields the η^2-complex $\mathbf{IN1_{AL}}$ upon π-coordination to the metal. The alkene in this η^2-complex may adopt four perpendicular conformations[13] relative to the Pd-C(alkenyl) vector, involving different orientations of the methyl bromide moiety.[14] Here we have only shown the conformation giving rise to the lowest-energy profile for the insertion, in which the $-CH_2Br$ rests on the opposite side of the ring and of the endocyclic oxygen. The π-coordination gives rise to symmetrical Pd-alkene bonds [Pd–C(H_2) 2.246 and Pd–C(H) 2.264 Å], and a lengthened C=C bond (Δ*d* 0.044 Å from the uncomplexed precursor to $\mathbf{IN1_{AL}}$). The formation of this η^2-complex is exothermic by $-7.5\ kcal\,mol^{-1}$. The coordinated alkene undergoes a 2,1-insertion into the Pd–alkyl bond in a stepwise process[15] that proceeds through the formation of a Pd complex $\mathbf{IN2_{AL}}$. This intermediate is formed via $\mathbf{TS1_{AL}}$, in which the four atoms forming new bonds (Pd–C 2.079 and C–C 2.097 Å) are roughly planar (deviation of 8.2°). Intriguingly, a *cis*/*trans* isomerization of the chloride ligand takes place to reach the transition state, probably in order to reduce the back-bonding interaction and to favor the Pd–C bond formation. A moderate activation barrier is found for this elementary step ($11.6\ kcal\,mol^{-1}$), the formation of the palladacyclobutane complex being favored from a thermodynamic viewpoint ($-9.7\ kcal\,mol^{-1}$).

The cycloalkene fragment in the Pd-complex $\mathbf{IN2_{AL}}$ still appears to be strongly, though asymmetrically, bound to the metal (Pd–C2 2.169, Pd–C3 2.232 Å), so the intermediate shows a distorted square-planar geometry around the metal with a vacant position *trans* to the new σ-Pd–C bond. The intermediate $\mathbf{IN2_{AL}}$ may then undergo a β-heteroatom elimination[16,17] to give the coupling product of type **7**, regenerating the active catalyst $PdCl_2$. Here, the liberated HCl plays a very important role in promoting the dehalopalladation and inhibiting the β-H elimination.[16g,18] It has been postulated that halide ions would assist the β-heteroatom elimination,

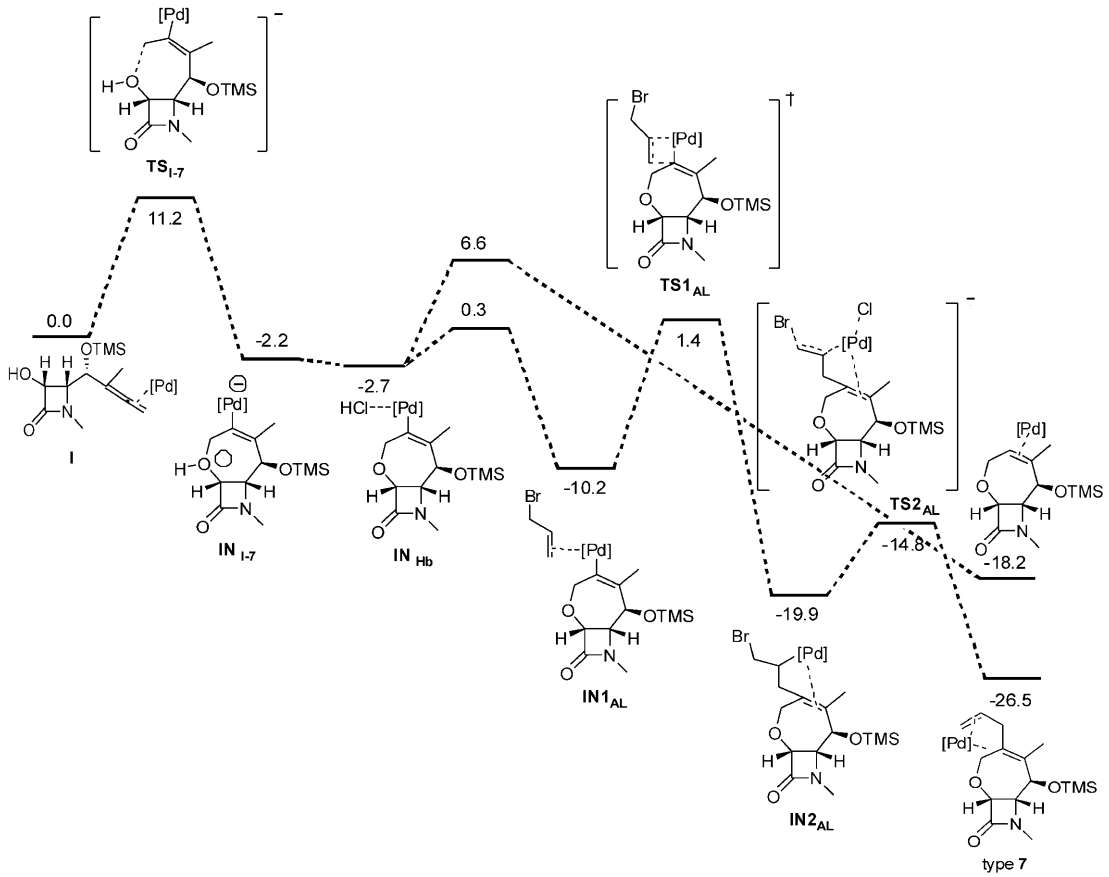

Figure 6. Free energy profile ($kcal\,mol^{-1}$) for the transformation of γ-allenol **I** into the tetrahydrooxepine of type **7**. Formation of the corresponding bicycle from protonolysis of the intermediate $\mathbf{IN_{Hb}}$ is shown for comparison.

through an E2-like mechanism promoted by halide ion coordination to Pd.[19] This *trans* β-elimination step takes place via $\mathbf{TS2_{AL}}$, in which the lengths of the forming and breaking bonds (2.481 Å for the Pd–Cl bond, 2.088 Å for the Br–C) on one hand, and enlargement of the Pd-alkene distance (2.703 and 3.205 Å) and advanced opening of the tetracycle (C-C-C 113.2°) indicate a large asynchronicity. The formation of the diene product thus proceeds in a final exothermic step by surmounting a low activation barrier (5.1 kcal mol^{-1}). Figure 7 shows the optimized structures for the olefin insertion and β-dehalopalladation processes. Alternatively, a *syn* β-dehalopalladation might be envisaged, in analogy with the β-H-elimination in related Pd^{II}-promoted processes.[20] Nevertheless, our computed results indicate that this pathway is less favored from a kinetic viewpoint because the transition structure on the pathway to the metalla-cyclobutane intermediate is 5.2 kcal mol^{-1} higher in energy that the equivalent for the alternative β-dehalopalladation (see the Supporting Information for details).

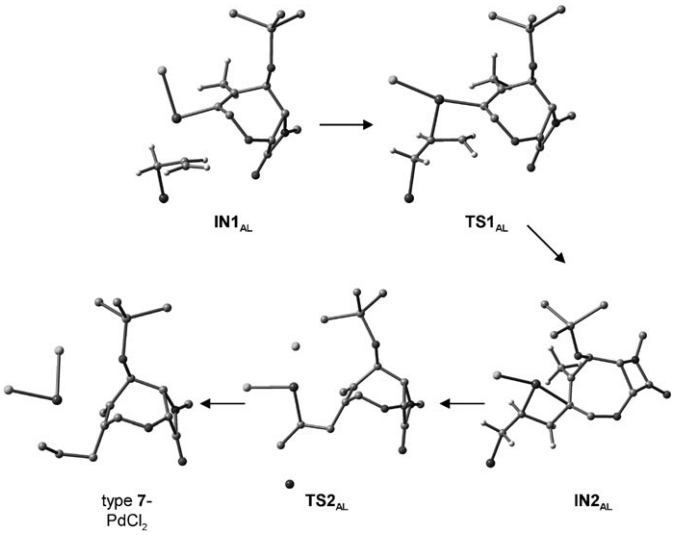

Figure 7. Optimized structures for the Pd^{II}–allyl coupling. Some H atoms have been omitted for clarity.

Scheme 3 outlines a proposed mechanistic explanation for the production of compounds of type **7**. Initial Pd^{II} coordination to the 1,2-diene moiety would give an allenepalladium complex $\mathbf{I}\cdot PdCl_2$. Species $\mathbf{I}\cdot PdCl_2$ would undergo an intramolecular cycloetherification reaction to give the intermediate palladatetrahydrooxepine $\mathbf{IN_{I\text{-}7}}$, which would react with allyl bromide via $\mathbf{IN_{1AL}}$ to form intermediate $\mathbf{IN_{2AL}}$. A *trans* β-heteroatom elimination would generate a tetrahydrooxepine-β-lactam of type **7** with concomitant regeneration of the Pd^{II} species (Scheme 3).

It is worth noting that the cyclization/coupling process affords cycloadducts **7** from 7-*endo-trig* cyclizations rather than from the kinetically preferred 5-*exo-trig* cyclization intermediates. This latter plausible mechanism, however, has been found to involve a highly congested transition structure

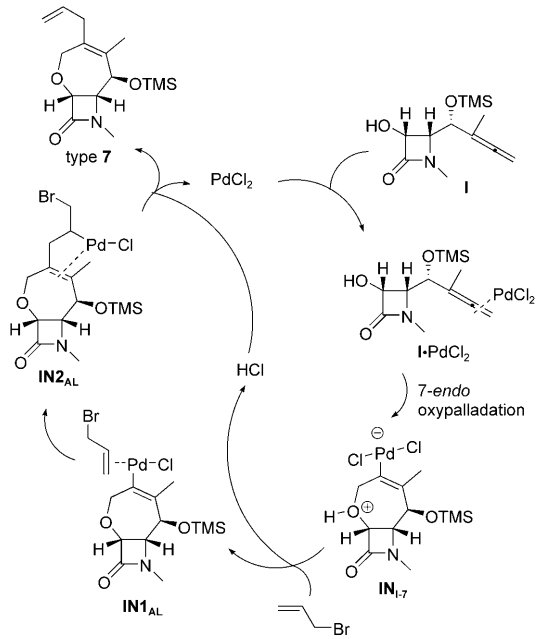

Scheme 3. Mechanistic explanation for the Pd^{II}-catalyzed heterocyclization of γ-allenol **I**.

for the olefin insertion (Figure 8), which accounts for the rather high activation barrier (25.4 kcal mol^{-1}) for this step, 14.8 kcal mol^{-1} higher than that from the seven-membered ring intermediate. Therefore, given that the cyclization and HCl formation are likely reversible processes under the reaction conditions, it could be argued that the kinetic preference for the coupling event from the seven membered-ring relative to other cyclic adducts and also to the protonolysis of the metal-carbon bond, along with the greater stability of the coupling product relative to the H-shift adduct, should funnel the reaction toward the observed product.

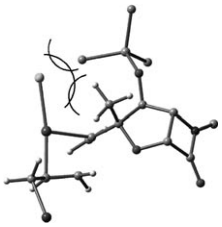

Figure 8. Transition structure for the alternative allyl-coupling with the 5-*exo* cyclized intermediate.

Protection of the α-hydroxy functionality with a MOM moiety has been shown to induce a different process when $AuCl_3$ is used as catalyst (Scheme 4 in Part 1, accompanying paper): γ-allenols **4** are transformed into dihydrofurans **10** by a chemoselective 5-*endo-trig* cyclization involving the ether protecting group. In view of these experimental findings, we carried out calculations on the γ-allenol model **II**; the optimized structures are depicted in Figure 9. In this case, the results suggest that the formation of the gold-dihydrofuran intermediate complex $\mathbf{IN_{II\text{-}5}}_{endo}$ is kinetic and thermodynamically favored over the competing 5-*exo-trig* and 7-*endo-trig* cyclization (Table 4).

The active participation of the protecting group as a nucleophilic entity is due to stereoelectronic and thermodynamic effects. The reaction takes place through a planarized

Table 4. Enthalpy and free energy differences in gas and in solution for the competing Au^{III}-catalyzed cyclization modes of γ-allenol **II**.

	ΔH	ΔG	ΔG_{sol}
II·$AuCl_3$	0.0	0.0	0.0
$\mathbf{TS_{II\text{-}5}}$	3.5	6.9	7.9
$\mathbf{IN_{II\text{-}5}}$	−3.4	−0.4	0.3
$\mathbf{TS_{II\text{-}7}}$	12.5	15.8	14.1
$\mathbf{IN_{II\text{-}7}}$	−1.8	1.0	−0.2
$\mathbf{TS_{II\text{-}5}}$*endo*	5.1	4.2	6.9
$\mathbf{IN_{II\text{-}5}}$*endo*	−2.9	−3.5	−12.7

five-membered cyclic transition structure, $\mathbf{TS_{II\text{-}5}}$*endo*, as is highlighted by the dihedral angle values (C1-C2-C3-C4 1.4°, C2-C3-C4-O −12.2°, C3-C4-O-C1 13.2, C4-O-C1-C2 11.5, O-C1-C2-C3 6.1°; see Figure 9). The metal lies in the C1-C2-C3 allene plane (0.8° in $\mathbf{TS_{II\text{-}5}}$*endo*, vs 6.1 and 17.8° in $\mathbf{TS_{II\text{-}5}}$ and $\mathbf{TS_{II\text{-}7}}$, respectively), which enhances the electrophilic activation of C1. The conformation in $\mathbf{TS_{II\text{-}5}}$*endo*, easily attained with small structural distortion from the reactant complex, allows an effective orbital overlap between the lone-pair orbital *n* and the π* orbital and charge transference to the electrophilic fragment, which results in a stabilization of the transition state relative to alternative routes. It should be noted that the bulky α-substituent in γ-allenol **I** would preclude effective interaction between the activated allene carbon and the oxygen atom. Additionally, as can be deduced from Table 4, the formation of the fused bicycle is associated with a less favored entropy contribution than in the case of the non-fused dihydrofuran ($\Delta S_{\neq}^{\mathbf{II\text{-}5}} = -7.9$, $\Delta S_{\neq}^{\mathbf{II\text{-}7}} = -11.2$, and $\Delta S_{\neq}^{\mathbf{II\text{-}5}endo} = +2.9$ cal mol^{-1} K^{-1}, respectively). This thus leads to a lower free energy of activation to achieve $\mathbf{TS_{II\text{-}5}}$*endo* than to achieve other transition structures. Also, it implies that the formation of $\mathbf{IN_{I\text{-}5}}$*endo* has a thermodynamic driving force greater than that corresponding to the transformation into the alkenyl palladium intermediates $\mathbf{IN_{II\text{-}5}}$ or $\mathbf{IN_{II\text{-}7}}$ (Figure 10).

From the results detailed above, the regioselectivities of Au^{III}-catalyzed cyclizations of γ-allenols **4** mainly depend on two factors: the electronic properties of the acceptor carbon atom of the allene induced by the catalyst, and the structural properties of the α-substituent.

In sharp contrast, protection of the γ-hydroxy group inhibits the 5-*exo* cyclization, the 7-*endo* mode now being the operative pathway, to yield fused tetrahydrooxepines **11** (Scheme 5 in Part 1, accompanying paper). To shed light on this result, we have explored both cyclization modes for precursor **III**. In this case, the calculations provide a clear picture and indicate that the 5-*exo-trig* cyclization transition structure $\mathbf{TS_{III\text{-}5}}$ is 5.1 kcal mol^{-1} less stable than the 7-*endo* cyclization intermediate $\mathbf{TS_{III\text{-}7}}$ because of strong steric effects. The intramolecular attack on the internal allenic carbon is inhibited by steric hindrance between the methoxymethyl group and the catalyst (Figure 11). A comparison with the preferential 5-*exo* transition structure of **I** ($\mathbf{TS_{I\text{-}5}}$) reveals that $\mathbf{TS_{III\text{-}5}}$ not only lacks the stabilizing H-bond interaction between the hydroxy group and the ligand catalyst found in $\mathbf{TS_{I\text{-}5}}$, but also shows a destabilizing steric interaction owing to the protecting group. The O–C3 distance in $\mathbf{TS_{III\text{-}5}}$ is shorter (2.384 Å) than in $\mathbf{TS_{I\text{-}5}}$ (2.457 Å), which further enhances the steric repulsion, as indicated by the deviation of the metal from the π plane (9.7 vs 0.1° in $\mathbf{TS_{I\text{-}5}}$) and the torsion of the C1-C2-C3-C4 angle (41.4 vs −7.1° in $\mathbf{TS_{I\text{-}5}}$). The transition structure is thus achieved with a higher structural distortion from ideal values. The subsequent alkenyl gold intermediate $\mathbf{IN_{III\text{-}5}}$ should be formed by opening of the C1-C2-C3-C4 dihedral angle as the O–C3 distance decreases, but this torsion would increase the strong steric congestion between the catalyst or the alkene fragment. In fact, the calculations reveal that $\mathbf{TS_{III\text{-}5}}$ evolves to a highly unstable uncyclized intermediate (O–C3 2.367 Å), only 0.01 kcal mol^{-1} more stable than $\mathbf{TS_{III\text{-}5}}$, so it must revert to the reactant Au complex, which funnels the reaction toward the formation of the tetrahydrooxepine.

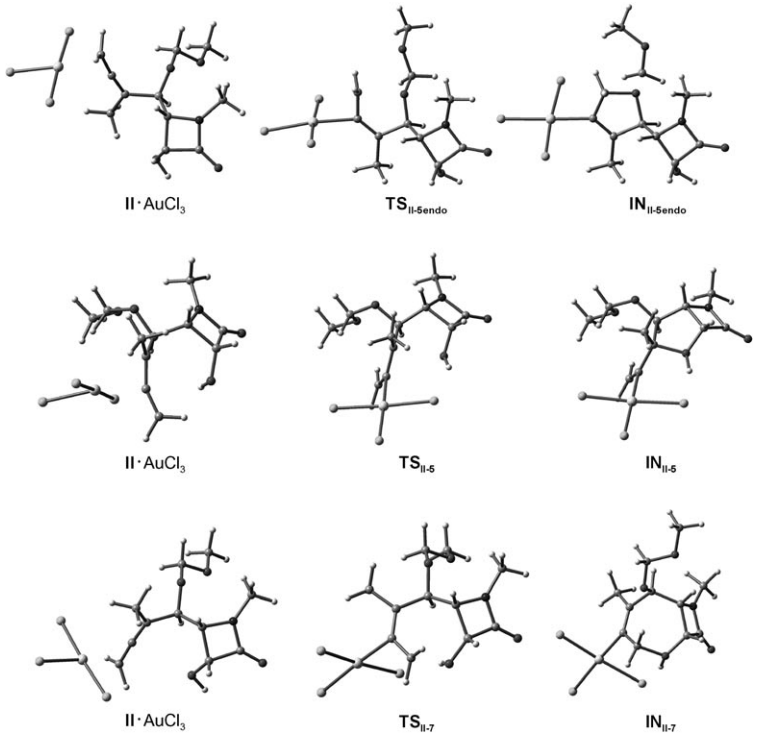

Figure 9. Optimized structures of the Au^{III}-catalyzed cyclization step of γ-allenol **II** by the competing 5-*endo-trig*, 5-*exo-trig*, and 7-*endo-trig* modes.

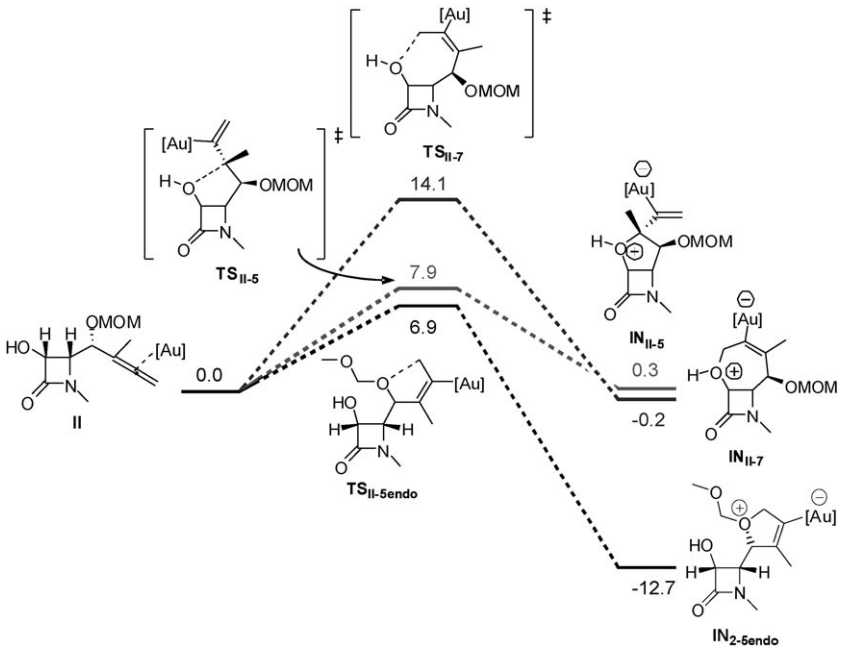

Figure 10. Free energy profile (kcal mol^{-1}) for the Au-catalyzed oxycyclization of γ-allenol **II** through alternative pathways.

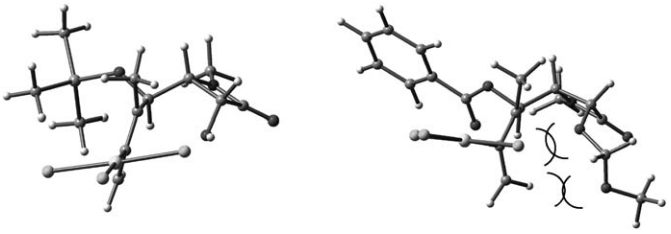

Figure 11. Comparison between the transition structures **TS$_{I-5}$** and **TS$_{III-5}$**.

The pathway proposed in Scheme 4 looks valid for the formation of products of type **11** from MOM-protected γ-allenol derivative **III**. It could be presumed that the initially formed allenegold complex **III**·$AuCl_3$ undergoes an intramolecular attack (7-*endo* versus 5-*exo* oxyauration) by the methoxymethyl group, giving rise not to species **IN$_{III-5}$** but to the tetrahydrooxepine intermediate **IN$_{III-7}$**. Protonolysis of the carbon-gold bond associated with an elimination of methoxymethanol would then liberate the bicycle type **11** with concomitant regeneration of the Au^{III} species. Probably, the proton in the last step of the catalytic cycle comes from trace amounts of water present in the solvent or the catalyst. In the presence of the MOM group, 5-*exo* cyclization falters. As calculations reveal, 5-*exo* oxyauration via **IN$_{III-5}$** is restricted by the steric hindrance between the methoxymethyl group and the substituents at the quaternary stereocenter.

With the aim of trapping the organogold intermediate to confirm the mechanism of this reaction, we performed deuterium labeling studies with deuterium oxide. Under otherwise the same conditions, but with the addition of two equivalents of D_2O, $AuCl_3$-catalyzed heterocyclization of MOM-protected γ-allenol **3e** (numbering of compounds consistently with Part 1, accompanying paper) in dichloromethane afforded [4-D]-**11a** in 48% yield, indicating that a deuterium atom was incorporated at the alkenyl carbon (Scheme 5). The fact that the $AuCl_3$-catalyzed conversion of allenol **3e** into bicycle **11a** in the presence of two equivalents of D_2O afforded [4-D]-**11a**—as judged from the disappearance of the peak at 6.35 ppm in the ^{1}H NMR spectrum, which is the signal of the 4-H proton in 2-oxa-8-azabicyclo[5.2.0]non-4-en-9-one (**11a**)—suggests that deuterolysis of the carbon-gold bond in species type **IN$_{III-7}$** has occurred. Along with the clarification of the reaction

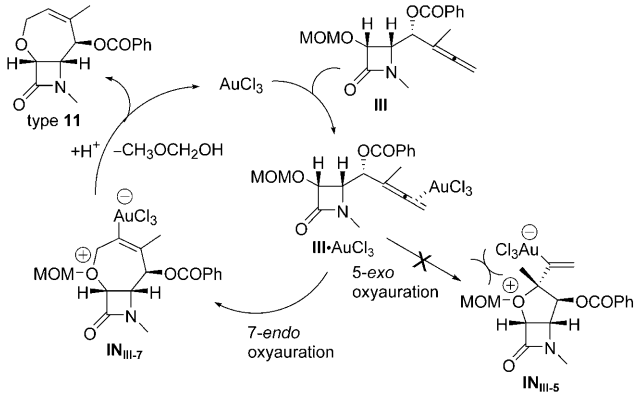

Scheme 4. Mechanistic explanation for the Au^{III}-catalyzed heterocyclization of MOM-protected γ-allenol derivatives **III**.

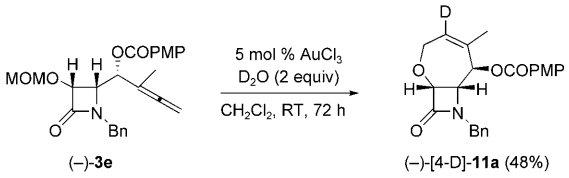

Scheme 5. Au^{III}-catalyzed heterocyclization of MOM-protected γ-allenol derivative **3e** (numbering of compounds consistently with Part 1, accompanying paper). Reagents and conditions: a) $AuCl_3$ (5 mol%), D_2O (2 equiv), CH_2Cl_2, RT; MOM = $MeOCH_2$, PMP = 4-$MeOC_6H_4$.

mechanism, we should at the same time point out that, although metal-catalyzed oxycyclization reactions of allenes are well known in the case of hydroxyallenes, heterocycliza-

tion of alkoxyallenes is not an easy task and still remains a real challenge.

The regioselectivities observed in organolanthanide-mediated hydrofunctionalization processes such as hydrophosphination, hydrosilylation, hydroboration, intermolecular hydroamination, and intramolecular hydroamination/cyclization differ markedly from those seen in the cases of most transition metal catalysts with similar substrates, which suggests a different activation mode and reaction mechanism. In this context, Marks et al. have carried out comprehensive kinetic and mechanistic studies that have led to a generally accepted mechanistic scenario for organolanthanide-catalyzed intramolecular hydroamination/cyclization.[21] It is characterized by the following features common to the various unsaturated C=C functionalities: 1) smooth precatalyst activation through protonolysis by the substrate, 2) a large negative activation entropy ($\Delta S^{\neq}$), suggesting a rather organized transition state, and 3) a reaction rate that is first order in [catalyst] and zeroth order in [substrate]. Similar conclusions have been also drawn for intramolecular hydroalkoxylation/cyclization when using $La[N(SiMe_3)_2]_3$ as precatalyst. In addition, labeling studies have suggested a nonprimary isotopic effect, which is consistent with the unsaturated C=C bond insertion being the turnover-limiting step.[22] These observations point to a mechanism through a slow insertion into the unsaturated moiety, followed by rapid substrate protonolysis. Computational work by Tobisch, however, has suggested that in the case of amino derivatives the protonolysis step is only slightly kinetically disfavored relative to the intramolecular C–N bond formation, accounting for the origin of the measured large negative $\Delta S^{\neq}$.[23]

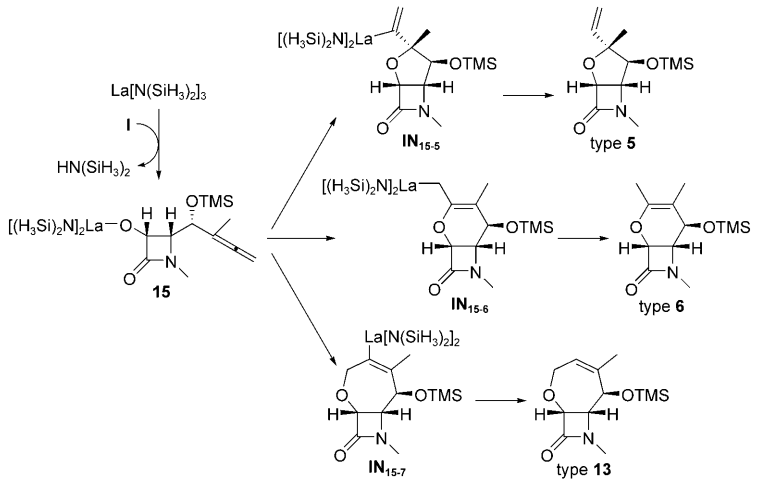

Scheme 6. Various cyclization modes (5-*exo*, 6-*exo*, and 7-*endo*) of γ-allenol **I** on organolanthanide-catalyzed hydroalkoxylation.

As can be deduced from experimental results (Schemes 1 and 6 in Part 1, accompanying paper)[3], the regioselectivities of the intramolecular hydroalkoxylations/cyclizations of γ-allenols **4** depend very much on the protecting group and allene substitution pattern. The catalytic cycle for the organolanthanide-mediated cyclohydroalkoxylation of allenol **I** is initiated by the precatalyst $La[N(SiH_3)_2]_3$, which is activated—through protonolysis—by substrate **I**, generating the catalytically active La-alkoxy complex species **15** and liberating the amine ligand (Scheme 6). The precatalyst activation proceeds through the early transition structure $\mathbf{TS_{PRE}}$, in which the acidic hydroxylic proton is still close to the oxygen atom (1.260 Å). The La–N distance with the leaving ligand is only slightly longer than that with the oxygen (2.296 vs. 2.248 Å, respectively). This proton transfer takes place with a moderately low activation barrier ($\Delta G^{\neq} =$ 12.3 kcal mol^{-1}) and is slightly exergonic (by −2.7 kcal mol^{-1}), thereby indicating a favorable transformation. The catalytically active structure **15** has relatively poor conformational freedom because of the β-lactam ring, although other conformers, readily interconvertible, may be envisaged as a function of the allene orientation; nevertheless, the η^1-allene complex (La–C1 = 3.103 Å; Figure 12) is thermodynamically more stable because of the coordinative saturation of the electrophilic La center by the π system. The geometry of the model precatalyst is found to be a tetrahedral arrangement around the La^{3+} ion. The allenic C=C linkage subsequently adds across the La–O functionality of catalyst complex **15** to afford cyclized intermediates. This addition can occur through 5-*exo*, 6-*exo*, or 7-*endo* cyclization pathways, giving rise to the regioisomeric five-, six-, and seven-membered intermediates $\mathbf{IN_{15\text{-}5}}$, $\mathbf{IN_{15\text{-}6}}$, and $\mathbf{IN_{15\text{-}7}}$, respectively (Scheme 6).

The overall energies involved in hydroalkoxylation/cyclization processes on passing from the acyclic substrates to the final cyclized products reveal that the processes are more exothermic for the dihydropyran derivative type **6** ($\Delta H_0 = -30.8$ kcal mol^{-1} vs. −17.8 for the tetrahydrofuran of type **5** and −15.5 kcal mol^{-1} for the tetrahydrooxepine derivative of type **13**). As can be deduced from the calculated atomic charges (Table 5), the lanthanide complex increases the charge density on the bonded oxygen, thus enhancing its nucleophilic character and preferentially promoting the intramolecular nucleophilic attack over the more electrophilic allene carbon atoms, C2 and C3.

In analogy with the results computed for the cyclizations catalyzed by late transition metals (Au^{III} and Pd^{II}; see above), these electronic data suggest that the reaction should preferentially proceed through 5-*exo* or 6-*exo* cyclization, so other factors must mediate to account for the observed structure-dependent regiochemistries. The optimized structures and energies for the alternative pathways are depicted in Figure 1. As can be observed, the 5-*exo* and 6-*exo*

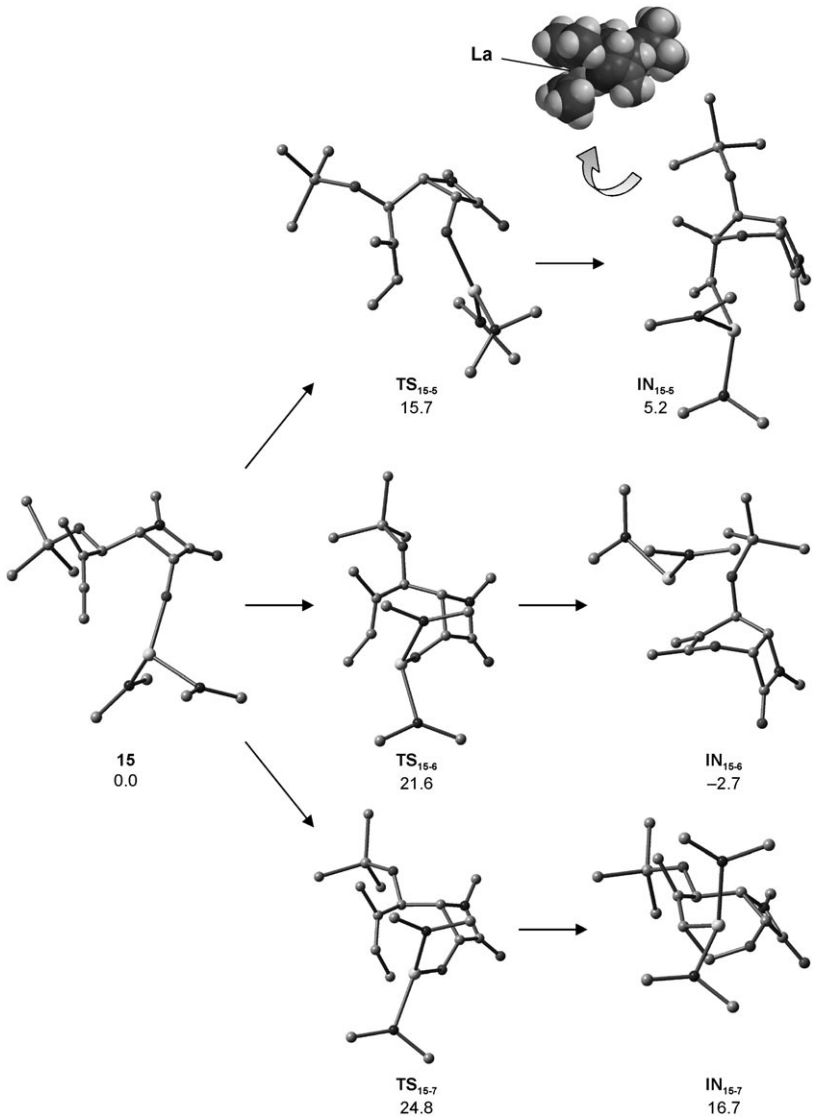

Figure 12. Optimized structures of the hydroalkoxylation/cyclization step of γ-allenol **I** in the competing 5-*exo*, 6-*exo*, and 7-*endo* modes. For $\mathbf{IN_{15\text{-}5}}$, the molecular structure with the van der Waals atomic radii is depicted. Free energy differences are given in kcal mol^{-1}. Hydrogen atoms have been omitted for the sake of clarity.

cyclization paths are kinetically more favorable than the 7-*endo* route, a trend consistent with the computed atomic charges. This La-catalyzed cyclization step therefore shows the same regioselectivity as that computed for the cyclization step mediated by late transition metals, although with the obvious differences in activation and mechanism. From a thermodynamic viewpoint, the formation of the dihydropyran intermediate ($\mathbf{IN_{15\text{-}6}}$) is slightly exothermic (by −2.7 kcal mol^{-1}), whereas the formation of the tetrahydrofuran intermediate ($\mathbf{IN_{15\text{-}5}}$) is endothermic (by 5.2 kcal mol^{-1}). The formation of the tetrahydrooxepine adduct ($\mathbf{IN_{15\text{-}7}}$) is largely endergonic (by 16.7 kcal mol^{-1}), which along with the unfavorable kinetics suggests that this would be an inoperative route. The 5-*exo* cyclization takes place through a *syn* addition of the metal and alkoxy units across the C=C double bond. Two alternative pathways can be envisioned, distinguished by the orientation of the allene-methyl substituent relative to the O-protecting group. In analogy with the results computed for the cyclization catalyzed by late transition metals, the 5-*exo* cyclization route should stereoselectively afford intermediate $\mathbf{IN_{15\text{-}5}}$, because the formation of its epimer at C3 takes place through the less stable transition structure $\mathbf{TS_{15\text{-}5}}'$ (5.6 kcal mol^{-1} higher in energy than $\mathbf{TS_{15\text{-}5}}$) in which the allene group adopts a *cis* orientation relative to the silyl ether moiety. This last conformation results in marked steric congestion arising from the protecting group and catalyst ligands. Steric effects can thus discriminate between the two 5-*exo* cyclization routes both kinetically and also thermodynamically, because $\mathbf{IN_{15\text{-}5}}$ is 7.4 kcal mol^{-1} lower in energy than $\mathbf{IN_{15\text{-}5}}'$.

In $\mathbf{TS_{15\text{-}5}}$ the La–O bond lengthens from the reactant state ($\Delta l = +0.313$ Å) to allow the formation of the incipient C–O (2.009 Å) and La–C2 (2.705 Å) bonds. This four-membered metallacycle is found to have a 4.9° folding angle. In this sense, it should be noted that the tension imposed by the β-lactam ring would favor the more restrained five-membered ring closing over larger heterocycles. $\mathbf{TS_{15\text{-}5}}$ evolves to the tetrahydrofuran intermediate $\mathbf{IN_{15\text{-}5}}$ (C–O 1.492, La–C2 2.606 Å), which notably displays a strong interaction be-

Table 5. NPA atomic charges on the reactant complex **15**. The charge for the uncomplexed precursor **I** is also shown, to illustrate the effect of the catalyst.[a]

	C1	C2	C3	C4	C5	C6	O	La	La[N(SiH$_3$)$_2$]$_2$
I	−0.480	+0.065	−0.103	+0.125	−0.020	+0.075	−0.758	+2.764	–
15	−0.624	+0.076	−0.067	+0.125	−0.019	+0.097	−1.160	+2.771	+0.913

[a] Calculated at the B3LYP/LANL2DZ level (see Computational Methods for details).

tween the metal and the lactam carbonylic oxygen atom (2.556 Å), already incipient in $\mathbf{TS_{15\text{-}5}}$ (2.692 Å). This structural element, although it most likely stabilizes the transition state, places the metal center shielded from other reactive groups in $\mathbf{IN_{15\text{-}5}}$ (see molecular structure constructed with the van der Waals atomic radii, Figure 12), which could inhibit the ensuing protonolysis event and explain the lack of the tetrahydrofuran scaffold from the reaction products, as we discuss later.

Similarly to what was computed for the Au^{III}- and Pd^{II}-catalyzed processes, the formation of the seven-membered ring intermediate $\mathbf{IN_{15\text{-}7}}$ proceeds with the highest activation barrier of the regioisomeric paths, the subsequent intermediate also being the least stable cycloadduct out of the possible regioisomers. Although electronic factors can account for the high barrier, the distorted structure of $\mathbf{IN_{15\text{-}7}}$ would explain the low thermodynamic stability. The metal center bonds both with the oxygen atom and with C2 in $\mathbf{IN_{15\text{-}7}}$, which obstructs the coplanar arrangement of the olefin substituents, that is, La and methyl moieties (torsion angle C_{methyl}-C3-C2-La 56.8°), whereas the ring-puckering changes (as in the case of $\mathbf{IN_{I\text{-}7}}$; see above) to relieve steric congestion due to the bulky protecting group in the cyclized adduct. Additionally, this arrangement enhances the steric repulsion between the methyl substituent and the protecting group.

Alternatively, a relaxed conformed $\mathbf{IN_{15\text{-}7}}'$ in which the lack of La–O interaction allows the coplanar rearrangement of the olefinic substituents has been located (Figure 13). However, this intermediate is only 1 kcal mol^{-1} more stable than $\mathbf{IN_{15\text{-}7}}$. The conformational rearrangement involves the relaxation and opening of the C3-C4-C5 bond angle and the concomitant closure of the angles C3-C4-O_{TMS} and C5-C4-O_{TMS}, thus giving rise to stronger steric repulsions between the protecting group and the lactam and C3 substituents (Figure 13).

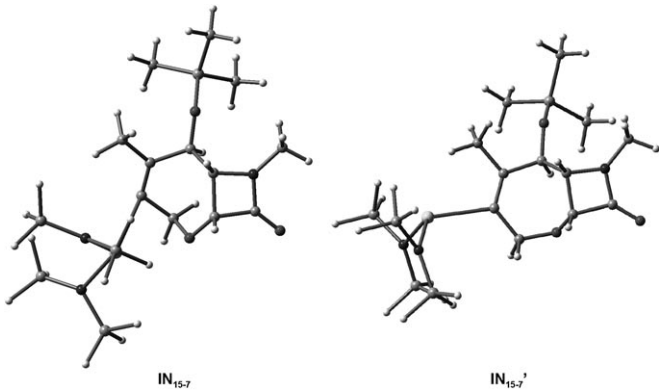

Figure 13. Optimized geometries of 7-*endo*-oxycyclized conformers.

In the 6-*exo* cyclization, the late transition structure $\mathbf{TS_{15\text{-}6}}$ (reached at the shortest C–O distance: 1.856 Å, vs. 2.009 and 2.067 Å for $\mathbf{TS_{15\text{-}5}}$ and $\mathbf{TS_{15\text{-}7}}$, respectively) is a nearly symmetric η^2-complex (C1–La 2.855; C2–La 2.810 Å). Ring closure through the 6-*exo* route is sterically demanding as a result of severe repulsive interactions between the methyl substituent and the catalyst backbone (Figure 12), thus making this pathway significantly more expensive kinetically than the 5-*exo* path. Remarkably, a ring-puckering change takes place to afford a boat-like cyclized intermediate, $\mathbf{IN_{15\text{-}6}}$, a conformation that allows the coordination, albeit weak, of the lanthanide complex to both ether moieties (La–O 2.973 and La–O_{TMS} 2.693 Å). This coordination mode, along with the η^3-allylic coordination (La–C1 2.777, La–C2 2.699, La–C3 2.928 Å), stabilizes the dihydropyran framework. Alternatively, the ring closure can proceed through the catalyst approaching *trans* to the OTMS group. However, this step is about 2 kcal mol^{-1} less favorable because of the lack of stabilizing interaction between the ether and the metal center. In summary, the kinetic preference for the formation of $\mathbf{IN_{15\text{-}5}}$ is likely due to electronic effects, whereas the thermodynamic preference for the formation of $\mathbf{IN_{15\text{-}6}}$ can be traced back to steric factors associated with the coordination mode of the catalyst. The evolution of each heterocyclic intermediate is thus decisive to account for the experimental results.

The cyclization is followed by a La–C protonolysis process, which regenerates the catalyst and releases the heterocyclic product. In this context it is possible to envision two possible pathways: i) protonolysis by γ-allenol **I**, which leads to the corresponding cycloadduct and regenerates **15**, thus reinitiating the catalytic cycle, or ii) protonolysis by the liberated amine, which ends the process and regenerates the precatalyst form. As suggested by the results shown in Figure 12, the thermodynamic population of $\mathbf{IN_{15\text{-}7}}$ is likely negligible, owing to the kinetically precluded, strongly endothermic 7-*endo* cyclization. As a consequence, the path for protonolysis to provide the tetrahydrooxepine product should remain blocked, irrespective of whether or not protonolysis is kinetically feasible. The discussion is therefore primarily focused on the favorable pathways for proton transfer for $\mathbf{IN_{15\text{-}5}}$ and $\mathbf{IN_{15\text{-}6}}$ intermediates.

A second substrate molecule (simulated here as 3-hydroxy-1-methylazetidin-2-one) coordinates to the lanthanum center to form the complex $\mathbf{IN_{P15\text{-}\mathit{n}}}$ prior to the proton transfer from the hydroxy group to the La species. Under these conditions, it would be expected that the larger the steric crowding around the metal center, the harder the transfer. This proton transfer step affords a La–O complex stabilized by coordinative interaction with the oxygen lone pair, which after dissociation regenerates the active catalyst. If the protonolysis of the five- and six-membered intermediates $\mathbf{IN_{15\text{-}5}}$ and $\mathbf{IN_{15\text{-}6}}$, respectively, is taken into account, the initial formation of the precursor adducts $\mathbf{IN_{P15\text{-}5}}$ and $\mathbf{IN_{P15\text{-}6}}$ is uphill at the ΔG surface because the pertinent enthalpic stabilization is not counterbalanced by the entropic penalty accompanying the bimolecular association. We therefore focus on the cyclization adduct as reference.

For the protonolysis of the external allyl position of $\mathbf{IN_{15\text{-}6}}$, the hydroxy group of the incoming substrate can freely accede to the coordination sphere around the metal center.

A transition-state structure, $\mathbf{TS_{P15\text{-}6}}$, representing simultaneous O–H bond cleavage and C–H bond formation in an asynchronous mode (1.161 vs. 1.406 Å) is encountered along the favorable path for the proton transfer. $\mathbf{TS_{P15\text{-}6}}$ evolves to the complexed product $\mathbf{P_{15\text{-}6}}$, from which the cyclic skeleton of type **6** is liberated in a kinetically facile displacement by the incoming **I**. The transition state energy for protonolysis relative to complex $\mathbf{IN_{15\text{-}6}}$ is 23.1 kcal mol^{-1} (20.4 kcal mol^{-1} relative to reactants; Figure 14), and the product, $\mathbf{P_{15\text{-}6}}$, is stabilized by 1.4 kcal mol^{-1} with respect to $\mathbf{IN_{15\text{-}6}}$ (4.1 kcal mol^{-1} relative to reactants). The accessible activation enthalpy ($\Delta H^{298}_{\ddagger} = 11.8$ kcal mol^{-1}) in the protonolysis step is consistent with a concerted transition state, with significant bond formation to compensate for simultaneous bond cleavage. The large, negative activation entropy ($\Delta S^{298}_{\ddagger} = -28.6$ cal mol^{-1}K^{-1}) is consistent with a highly organized transition state in which a significant loss of internal degrees of freedom occurs from a bimolecular association. Release of the heterocyclic products by complex dissociation is an exothermic process. The overall transformation from **I** into bicycle type **6** is exothermic, driven by a thermodynamic force of $-30.8/-28.9$ mol^{-1} ($\Delta H/\Delta G$).

Alternatively, we explored the protonolysis of the 5-*exo* cyclization intermediate $\mathbf{IN_{15\text{-}5}}$. The regioisomeric pathway for protonation to afford $\mathbf{IN_{15\text{-}6}}$ is predicted to be distinctly impeded kinetically because the access of the external alcohol to the metal center is complicated by the moderately strong interaction with the carbonyl oxygen of the amide moiety in $\mathbf{IN_{15\text{-}5}}$ (Figure 12). This intermediate is found to have a pseudotetrahedral architecture around the La^{3+} ion, with alkenyl and carbonyl moieties as ligands (La–C2 = 2.606 and La–O = 2.556 Å), so an efficient approach by the alcohol must take place on the opposite side to the La–O interaction and must be accompanied by a conformational rearrangement around the metal, which should indeed weaken the carbonyl interaction. In addition, the methyl substituent at C3 and the terminal alkene carbon C1 also exert strong steric hindrance. The activation energy to reach transition state $\mathbf{TS_{P15\text{-}5}}$ is therefore high (25.9 kcal mol^{-1} from $\mathbf{IN_{15\text{-}5}}$, 31.1 kcal mol^{-1} relative to reactants), this structure being >10 kcal mol^{-1} less stable than $\mathbf{TS_{15\text{-}6}}$ for the competing formation of the dihydropyran type **6**.

The protonolysis of diastereomeric $\mathbf{IN_{15\text{-}5}'}$ was also considered, but the attack of the alcohol is predictably inhibited by the bulky protecting group (activation barrier of 30.4 kcal mol^{-1} from $\mathbf{IN_{15\text{-}5}'}$) or, alternatively, by the terminal alkene carbon C1 (activation barrier of 28.2 kcal mol^{-1} from $\mathbf{IN_{15\text{-}5}'}$), depending on the approaching mode. Consequently, these findings suggest that, whereas a 5-*exo* mode would be the preferred cyclization pathway from a kinetic viewpoint, the ensuing protonolysis step is inhibited by severe steric congestion around the reactive centers on the cyclized intermediate. These results show an overall kinetic preference for the competing formation of the six-membered ring adduct type **6**, which has a thermodynamic driving force greater than that corresponding to the transformation of γ-allenol **I** into bicycle type **5**. With regard to the second conceivable protonolysis mode—that is, protonolysis by the li-

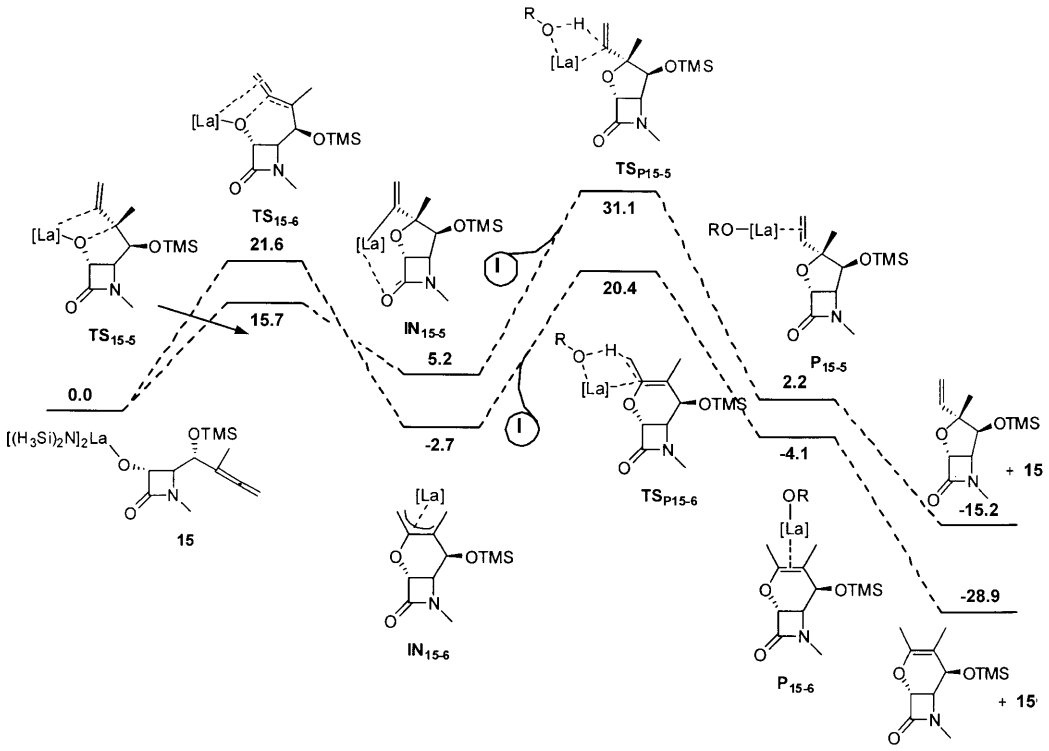

Figure 14. Free energy profile (kcal mol^{-1}) of the intramolecular hydroalkoxylation/cyclization of La-alkoxy complex **15** to give the tetrahydrofuran of type **5** and the tetrahydropyran of type **6**.

berated amine, thus ending the process and regenerating the homoleptic lanthanide amide precatalyst—the pertinent transition structure (N–H = 1.213, C–H = 1.378 Å) is only 1.2 kcal mol^{-1} less stable than that found for the alternative mode. Consequently, this path cannot be ruled out as an operative mechanism.

Scheme 7 shows a mechanistic rationale for the La[N(SiH$_3$)$_2$]$_3$-promoted conversion of methyl γ-allenol **I** into the fused tetrahydropyran of type **6**. Firstly, lanthanum precatalyst would form the alkoxide–La compound **15** through protonolysis at the La-[N(SiH$_3$)$_2$]$_3$ bond by allenol **I**. Subsequently, one π bond of the oxallene-La complex would regiospecifically add across the La–O functionality of **15** to afford oxacyclic intermediate **IN$_{15\text{-}6}$** by 6-*exo* cyclization to the central allene carbon. The intervention of a second molecule of allenol **I** would facilitate the proton-transfer step to afford species **P$_{15\text{-}6}$** via transition state **TS$_{P15\text{-}6}$**, which after dissociation would deliver the oxacycle of type **6** and regenerate **15**, thus reinitiating the catalytic cycle.

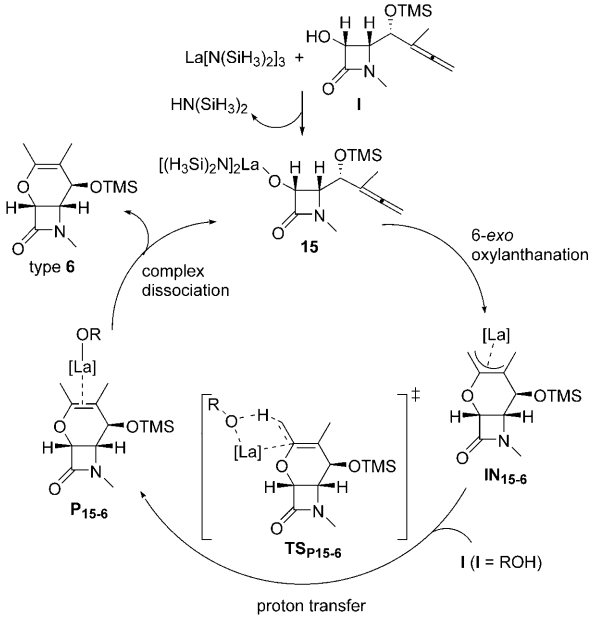

Scheme 7. Mechanistic explanation for the La^{III}-catalyzed heterocyclization of methyl γ-allenol **I**.

A rather different regiochemical outcome is experimentally found for MOM-protected γ-allenols (Scheme 6 in Part 1, accompanying paper). The allenol **4b** is transformed exclusively into the unprotected tetrahydrooxepine **13** in a regioselective 7-*endo* cyclization under the lanthanide amide conditions. In view of these experimental findings, we carried out calculations on the La complex **16**, formed through protonolysis by γ-allenol **II**. The computed free energy profiles for the cyclization step by the possible modes (Scheme 8) show the same trend as seen for **15**: that is, the 5-*exo* cyclization and 6-*exo* cyclization paths are kinetically and thermodynamically more favorable than the 7-*endo* route (Figure 15), in disagreement with the experimental evidence. The optimized structures are depicted in Figure 15. These results led us to suppose that the elimination of the protecting group might take place before the cyclization event, thus relaxing the reactant complex structure and favoring the formation of the larger seven-membered adduct over alternative pathways. Nevertheless, the calculations predict that the unprotected complex **17** should undergo a 7-*endo* cyclization by surmounting an energy barrier of 23.1 kcal mol^{-1}, only 0.5 kcal mol^{-1} lower than that computed for the parent model **16**.

As we have described above, the strained 7-*endo* cyclized intermediate can undergo a conformational rearrangement to a rotamer lacking La–O interaction, allowing the coplanar rearrangement of the olefinic substituents. Unlike in the case of **15**, this conformational relaxation to **IN$_{16\text{-}7}$′** gives rise to a stabilization of 7.6 kcal mol^{-1} in relation to **IN$_{16\text{-}7}$** because the protecting group is positioned without steric repulsions after the opening of the C3-C4-C5 and the closure of the C3-C4-O$_{MOM}$ and C5-C4-O$_{MOM}$ bond angles in **IN$_{16\text{-}7}$′** (Figure 16). Moreover, this σ–η^1 complex shows a suitable, unhindered, geometry around the reactive points for the subsequent attack of the alcohol in the protonolysis step. To address this question conveniently, we computed the energetics of the protonolysis step for the proposed intermediates **IN$_{16\text{-}5}$**, **IN$_{16\text{-}6}$**, and **IN$_{16\text{-}7}$**.

The calculations predict that the tetrahydrofuran framework should undergo a protonolysis showing an energy bar-

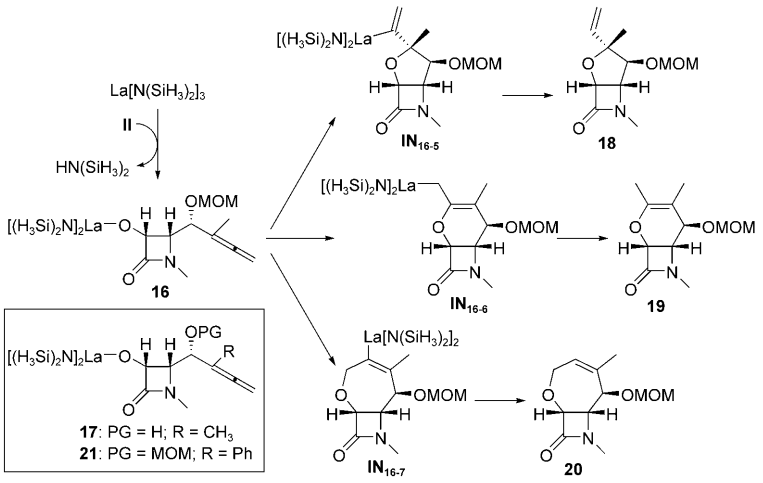

Scheme 8. Various organolanthanide-catalyzed hydroalkoxylation cyclization modes (5-*exo*, 6-*exo*, and 7-*endo*) of MOM-protected γ-allenol **II**.

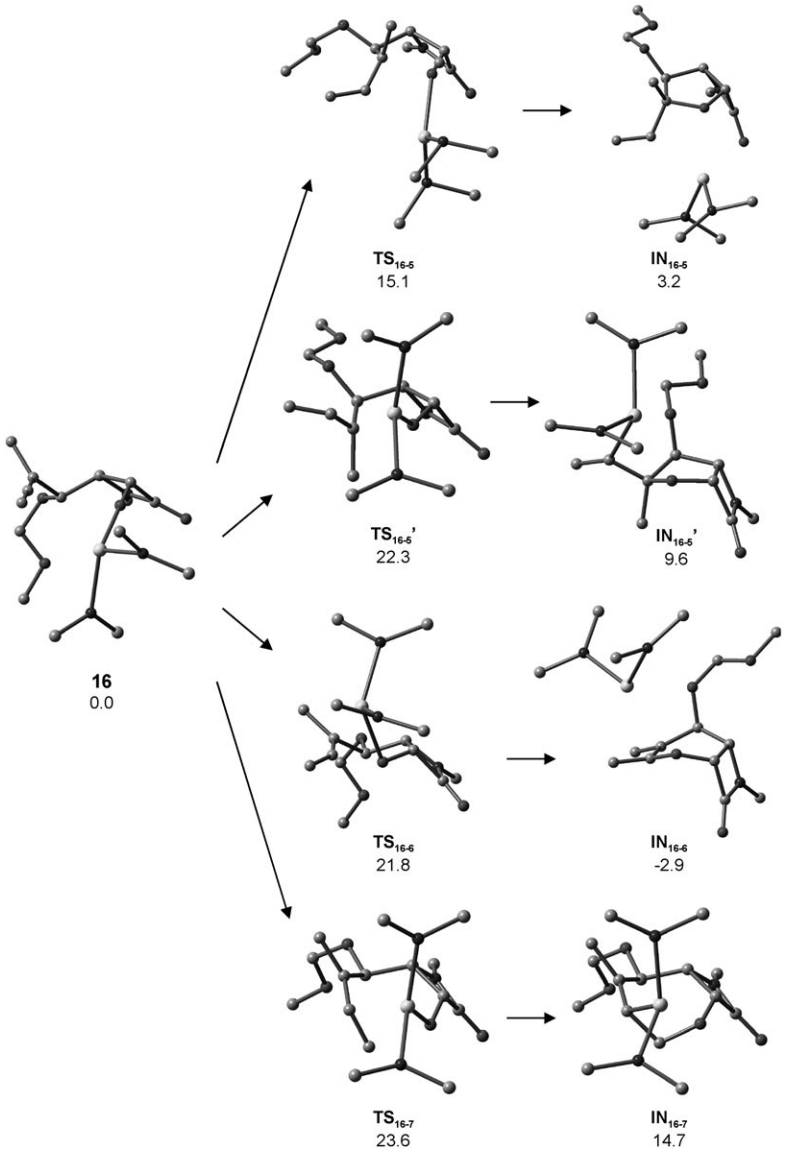

Figure 15. Optimized structures in the hydroalkoxylation/cyclization of γ-allenol **II** by competing 5-*exo*, 6-*exo*, and 7-*endo* modes. Free energy differences are given in kcal mol^{-1}. Hydrogen atoms have been omitted for the sake of clarity.

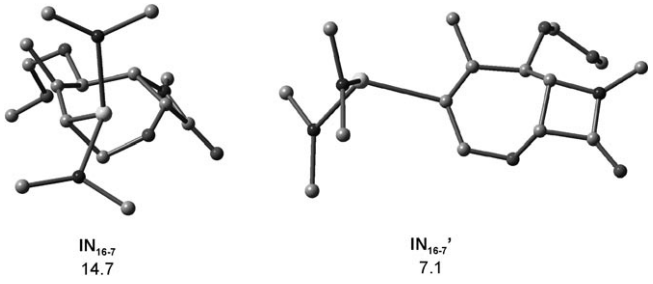

Figure 16. Optimized geometries of 7-*endo* oxycyclized conformers $\mathbf{IN_{16\text{-}7}}$ and $\mathbf{IN_{16\text{-}7}'}$.

rier similar to that seen for the silylated derivative (Figures 17 and 18), while the dihydropyran η^3-complex should undergo a slightly less favorable protonolysis, due to the stronger La–O_{OMOM} interaction in $\mathbf{IN_{16\text{-}6}}$ (2.654 vs. 2.692 Å in $\mathbf{IN_{15\text{-}6}}$), which provides a less electrophilic metal center for subsequent interaction with allenol **II**. As would be expected, the tetrahydrooxepine skeleton follows the kinetically more accessible protonolysis because of the decreased repulsive steric interactions between the incoming allenol and the La-σ–η^1 complex. The allenol can interact with the La–C bond through an unhindered tilted approach to the π plane of $\mathbf{IN_{16\text{-}7}'}$ (Figure 17).

The steric pressure therefore raises the protonolysis barrier and inhibits the formation of **18** and **19** in favor of the less obstructed tetrahydrooxepine adduct **20**. In summary, these data suggest that the cyclization event is sensitive to electronic and steric factors in the alkoxycyclization, but that the protonolysis process is even more dependent on steric effects as a result of the substituents on more compact and congested intermediate structures. This would account for the different mechanistic schemes postulated by Marks,[21] who defended a rate-limiting intramolecular C–C insertion into the lanthanide-heteroatom bond, and Tobisch,[24] who claimed a turnover-limiting protonation of the cyclized intermediate for related hydroamination/cyclization processes.

The proposed catalytic cycle for the La[$N(SiH_3)_2]_3$-catalyzed conversion of γ-allenol **II** into fused tetrahydrooxepine **20** is depicted in Scheme 9. Initially, lanthanum precatalyst would form the alkoxide-La compound **16** through protonolysis at the La–[$N(SiH_3)_2]_3$ bond by allenol **II**. Next, the distal π bond of the oxallene-La complex would regiospecifically add across the La–O functionality of **16** to afford tetrahydrooxepine intermediate $\mathbf{IN_{16\text{-}7}'}$ by 7-*endo* cyclization. The intervention of a second molecule of allenol **II** would facilitate the proton-transfer step to afford species $\mathbf{P_{16\text{-}7}}$ via transition state $\mathbf{TS_{P16\text{-}7}}$, which after dissociation would deliver oxacycle **20** and regenerate **16**, thus reinitiating the catalytic cycle.

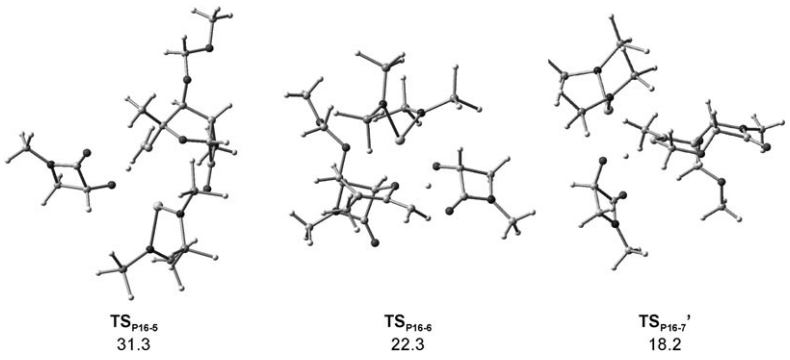

Figure 17. Optimized transition structures for the protonolysis step.

In sharp contrast, the lanthanum-catalyzed reaction of the related phenyl-allene **4e** affords the strained tricycle **14** in high yield, with dihydropyran **6b** as a minor product (Scheme 6 in Part 1, accompanying paper). Thus, through a subtle variation in the substitution pattern of the allene component (Ph vs. Me) the preferential formation of the seven-membered regioisomer can be reversed. To account for this unexpected result, it might be envisaged that electronic factors could come into play, because the electron-withdrawing phenyl substituent could enhance the electrophilicity of the benzylic carbon relative to the electron-donating methyl group, therefore favoring the 5-*exo* over the 7-*endo* cyclization. However, the calculated electronic properties, such as atomic charges, for the reactant La-complexes **16** and **21** (Scheme 8) appear similar for both γ-allenols (Table 6), hence pointing to parallel electrophilicity of the allene carbon C3. The difference in reactivity thus likely arises from steric effects. Under these circumstances, the sterically more demanding *C*-phenyl group might drive the reaction through a divergent mechanistic channel.

The formation of the tricyclic skeleton indicates the initial formation of the 5-*exo* cyclized adduct, which, as has been shown above, is the kinetically preferred cyclization route. As would be expected, the computed results once again predict the same trend as seen before for **15** and **16**: a kinetically favored 5-*exo* cyclization. The activation barriers are slightly higher than those predicted for the simpler model **16** because of the steric effects arising from the allene substituent: the transition structures for the 7-*endo* and 6-*exo* cyclizations—**TS$_{21-7}$** and **TS$_{21-6}$**, respectively—show the phenyl plane moderately deviating from the π plane of the bounded unsaturated C=C group (27 and 23°) to alleviate steric repulsions with the protecting group and catalyst ligands.

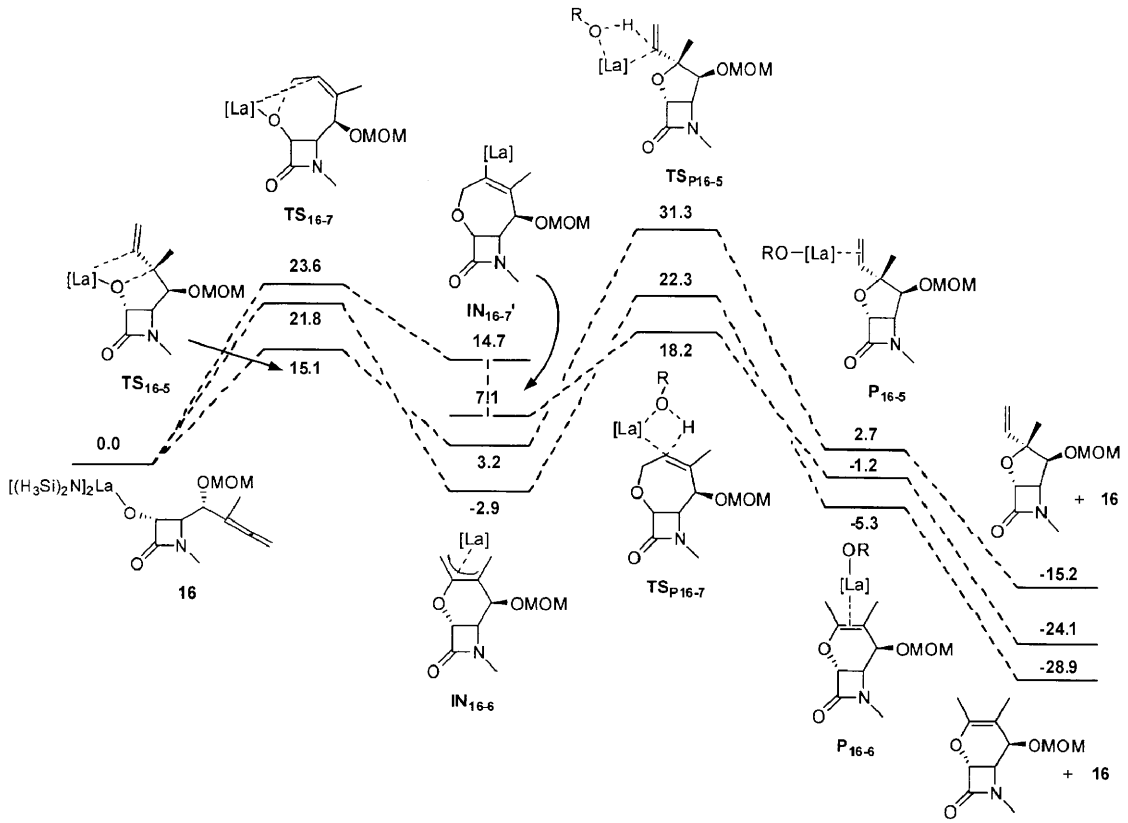

Figure 18. Free energy profile (kcal mol^{-1}) of the intramolecular hydroalkoxylation/cyclization of La–alkoxy complex **16**. Some structures have been omitted for the sake of clarity.

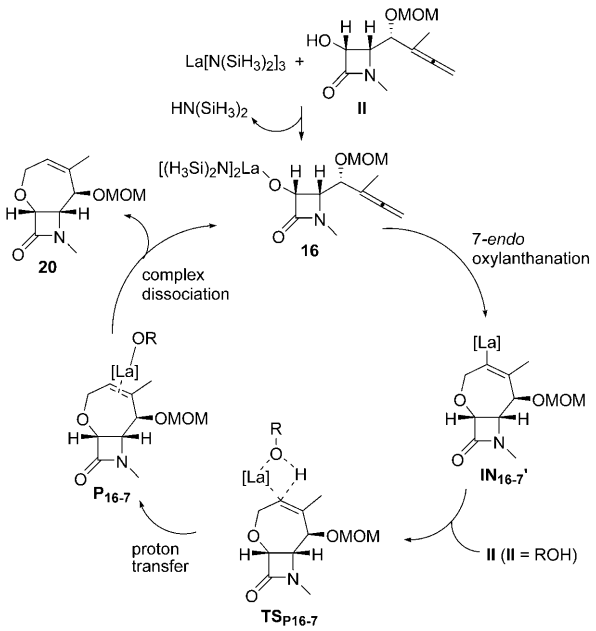

Scheme 9. Mechanistic explanation for the La^{III}-catalyzed heterocyclization of γ-allenol **II**.

These effects are probably responsible for the slightly increased energy barriers.

A better stabilization of the η^3-allyl lanthanide complex $\mathbf{IN_{21\text{-}6}}$, probably as a consequence of a weak La–phenyl interaction, should also be noted. For **21**, on the other hand, the 5-*exo* cyclization through a *trans* orientation of the allene moiety relative to the protecting group (through $\mathbf{TS_{21\text{-}5}}$) involves an energy barrier about 1 kcal mol^{-1} higher than in **16** because of the steric pressure caused by the allene substituent, whereas the cyclization through a *cis* orientation (through $\mathbf{TS_{21\text{-}5}'}$) is kinetically more accessible than in the analogous case for **16**. The transition state is reached earlier for **21** than for **16**, as suggested by the forming bond lengths (1.995 for $\mathbf{TS_{21\text{-}5}'}$ and 1.970 Å for $\mathbf{TS_{16\text{-}5}'}$). This divergent trend stems from the steric repulsion between the aromatic ring and the alkoxy oxygen, which induces the opening of the dihedral angle C3-C4-C5-C6 (−33.9° for $\mathbf{TS_{21\text{-}5}'}$, −0.2° for $\mathbf{TS_{16\text{-}5}'}$), thus allowing a moderate stabilizing La–O_{OMOM} interaction (2.943 for $\mathbf{TS_{21\text{-}5}'}$, 4.772 Å for $\mathbf{TS_{16\text{-}5}'}$) (Figure 19). These observations indicate that the steric effects introduced by the phenyl group are able to lead to significant changes in the position of the transition state on the reaction coordinate.

With regard to the protonolysis step, the computed energy profiles (Figure 20) reveal higher barriers for the six- and seven-membered heterocycles than for the parent precursor **16** because of the steric obstruction from the phenyl substituent to the incoming H-donor. As would be expected, this effect is stronger for $\mathbf{TS_{P21\text{-}7}}$ (energy barrier increased by 14 kcal mol^{-1}) than for $\mathbf{TS_{P21\text{-}6}}$ (energy barrier increased by 5 kcal mol^{-1}), due to the disposition of the aromatic ring with respect to the metal center and the approaching H-donor. In contrast, the five-membered ring intermediate undergoes a protonolysis process showing similar energy barriers (*cis* and *trans*) to those for **16**.

Overall, these results suggest the preferential formation of the dihydropyran skeleton, which disagrees with the experimental evidence because that was found as a minor product. The formation of the tricyclic framework of type **14** might proceed through the paths depicted in Scheme 10. By the postulated pathway a, a protonolysis step of the inter-

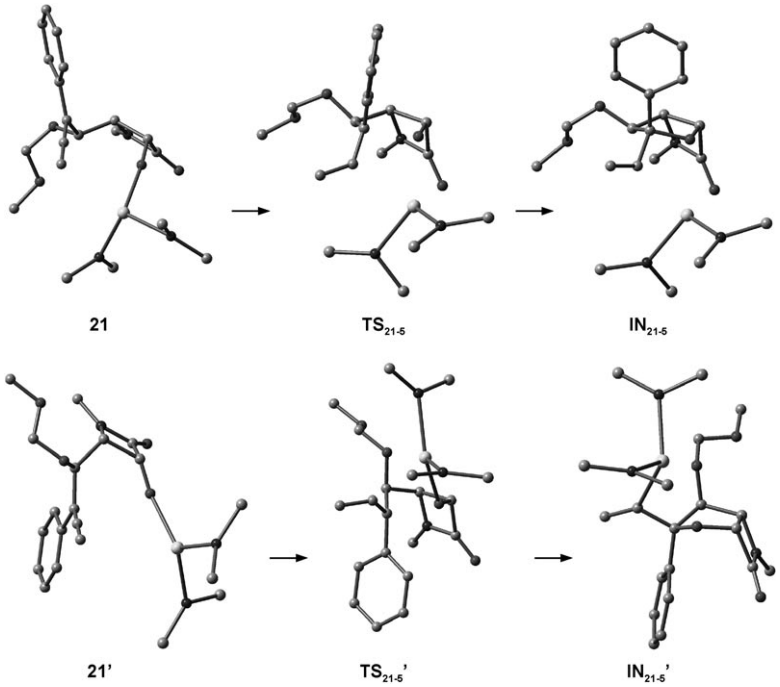

Figure 19. Optimized geometries of 5-*exo* oxycyclization.

Table 6. NPA atomic charges on the reactant complexes **16** and **21**.[a]

	C1	C2	C3	C4	C5	C6	O	La	$La[N(SiH_3)_2]_2$
21	−0.612	+0.077	−0.079	+0.092	−0.021	+0.100	−1.158	+2.768	+0.914
16	−0.588	+0.092	−0.106	+0.103	−0.023	+0.101	−1.155	+2.762	+0.911

[a] Calculated at the B3LYP/LANL2DZ level (see Computational Methods for details).

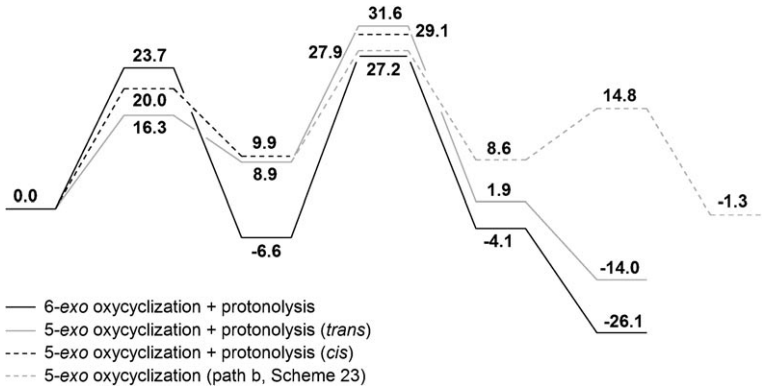

Figure 20. Free energy profile (kcal mol^{-1}) of potential intramolecular hydroalkoxylation/cyclizations of La-alkoxy complex **21**.

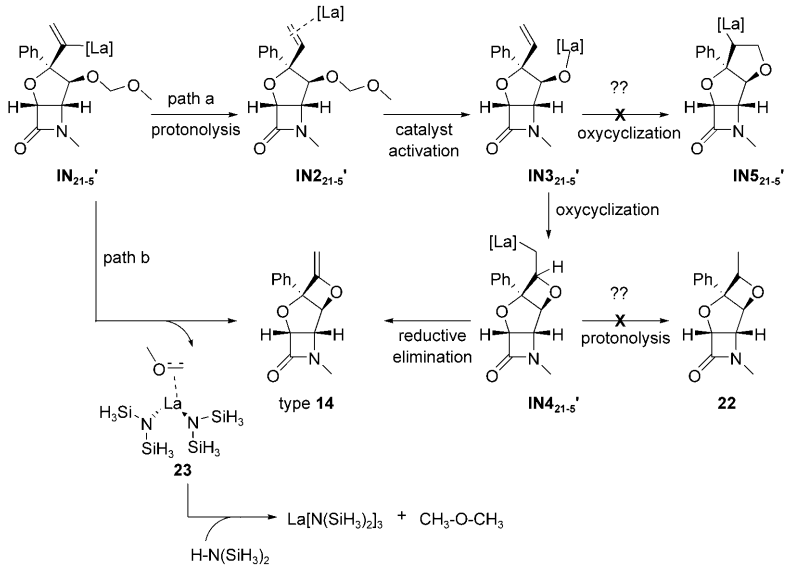

Scheme 10. Proposed modes of formation of tricycle type **14** by two alternative pathways.

mediate $\mathbf{IN}_{21\text{-}5}'$ would yield the coordinated alkene $\mathbf{IN2}_{21\text{-}5}'$, which might undergo a subsequent 4-*exo* oxycyclization to $\mathbf{IN4}_{21\text{-}5}'$ through catalyst activation via $\mathbf{IN3}_{21\text{-}5}'$. Predictably, the formation of $\mathbf{IN2}_{21\text{-}5}'$ and $\mathbf{IN3}_{21\text{-}5}'$ takes place with energy barriers lower than for the formation of $\mathbf{IN}_{21\text{-}5}'$, hence supporting this path as an operative route. Nevertheless, two disappointing questions now arise. Firstly, $\mathbf{IN4}_{21\text{-}5}'$ could undergo an easy protonolysis to afford **22**, because the reactive centers are unhindered to the incoming H-donor structure, whereas the lanthanide-assisted elimination of the olefinic proton to yield compound type **14** would involve higher steric pressure.

Secondly, $\mathbf{IN3}_{21\text{-}5}'$ could evolve through a 5-*endo* oxycyclization to deliver a less strained five-membered ring intermediate $\mathbf{IN5}_{21\text{-}5}'$. Theoretical studies have found a preference for *exo* cyclization over its *endo* counterpart (in general to yield 5- rather than 6-cyclized adducts) for a variety of unsaturated precursors and have concluded that *endo* cyclization is not seen to benefit from a coordinative stabilization of the metal center by the exocyclic group.[23–25] However, the 5-*endo* cyclization under study could gain from a smaller annular tension in relation to the 4-*exo* route. Indeed, the computed energy profiles for the two processes reveal a slight kinetic preference (by 1.1 kcal mol^{-1}) for the formation of $\mathbf{IN5}_{21\text{-}5}'$.

These results led us to propose *pathway b*, in which a 4-*exo* oxyclization directly affords tricycle type **14** and the La complex **23**. Ensuing protonolysis, kinetically very accessible, regenerates the precatalyst structure and liberates dimethyl ether as by-product. This pathway is structurally characterized in Figure 21. As a result of the steric repulsions produced by the phenyl substituent, the initial oxycyclization to $\mathbf{IN}_{21\text{-}5}'$ places the reactive centers close enough (2.714 Å) to ensure a minor geometric rearrangement to achieve the transition state $\mathbf{TS}_{\mathbf{C21\text{-}5}}'$ (C–O 2.120 Å). The computed atomic charges reveal a higher value for the O atom (−0.678) and a lower one for the C2 atom (−0.586) than observed in the initial complex **21** (Table 6), although the energy barrier value appears slightly higher than that for an alternative path (protonolysis of the 6-*exo* cyclization adduct). This mechanism would be favored over other conceivable routes (Scheme 10) and it accounts for the competing formation of the tricyclic framework over other five- and seven-membered ring adducts.

A conceivable catalytic cycle to account for the La[N(SiH$_3$)$_2$]$_3$-catalyzed formation of tricycle type **14** is proposed in Scheme 11.

Conclusion

In summary, an efficient metal-controlled regiodivergent preparation of bicyclic tetrahydrofurans, dihydropyrans, and tetrahydrooxepines, also bearing β-lactam moieties, from starting enantiopure γ-allenols has been developed. These are key structural motifs in biologically relevant compounds such as antibiotics and enzyme inhibitors. Theoretical work directed towards the elucidation of the mechanisms of the gold-, palladium-, and lanthanum-catalyzed oxycyclizations

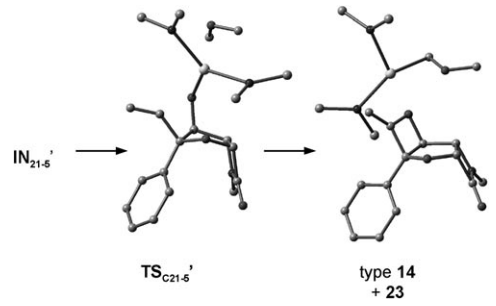

Figure 21. Optimized geometries for the final oxycyclization to the tricyclic product.

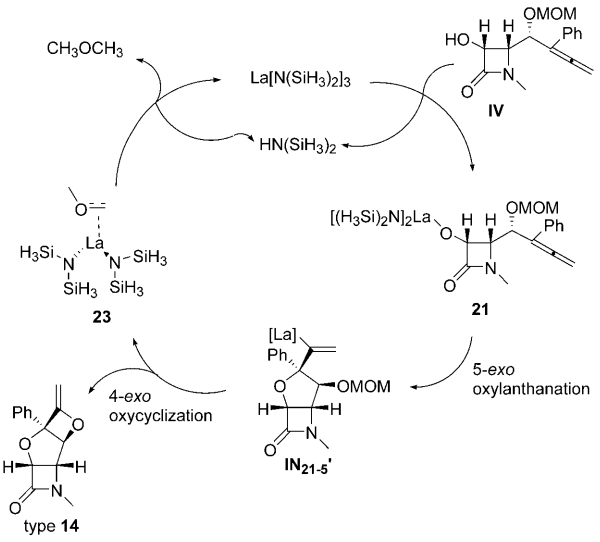

Scheme 11. Mechanistic explanation for the La^{III}-catalyzed heterocyclization of γ-allenol **IV**.

has been pursued in closed relationship with the experimental study (Part 1, accompanying paper) and has corroborated the bench results to provide a complete study of the reactivity of γ-allenols.

Acknowledgement

Support for this work by the DGI-MEC (CTQ2006-10292), the Comunidad Autónoma de Madrid (CCG-07-UCM/PPQ-2308), and the Universidad Complutense de Madrid (Grant GR74/07) is gratefully acknowledged. T.M.C. thanks the MEC for a predoctoral grant.

[1] For general and comprehensive reviews, see: a) S. Ma, *Chem. Rev.* **2005**, *105*, 2829; b) *Modern Allene Chemistry* (Eds.: N. Krause, A. S. K. Hashmi), Wiley-VCH, Weinheim, **2004**; c) R. Zimmer, C. U. Dinesh, E. Nandanan, F. A. Khan, *Chem. Rev.* **2000**, *100*, 3067.

[2] For selected reviews, see: a) R. A. Widenhoefer, *Chem. Eur. J.* **2008**, *14*, 5382–5391; b) N. Bongers, N. Krause, *Angew. Chem.* **2008**, *120*, 2208; *Angew. Chem. Int. Ed.* **2008**, *47*, 2178; c) R. A. Widenhoefer, X. Han, *Eur. J. Org. Chem.* **2006**, 4555; d) A. Hoffmann-Röder, N. Krause, *Org. Biomol. Chem.* **2005**, *3*, 387; e) S. Ma, *Acc. Chem. Res.* **2003**, *36*, 701; f) R. W. Bates, V. Satcharoen, *Chem. Soc. Rev.* **2002**, *31*, 12; g) A. S. K. Hashmi, *Angew. Chem.* **2000**, *112*, 3737; *Angew. Chem. Int. Ed.* **2000**, *39*, 3590.

[3] For Part 1, see preceding paper: B. Alcaide, P. Almendros, T. Martínez del Campo, E. Soriano, J. L. Marco-Contelles, *Chem. Eur. J.* **2009**, *15*, 1909–1928.

[4] For a preliminary communication, see: B. Alcaide, P. Almendros, T. Martínez del Campo, *Angew. Chem.* **2007**, *119*, 6804; *Angew. Chem. Int. Ed.* **2007**, *46*, 6684.

[5] Gaussian 03, Revision B.03, M. J. Frisch, G. W. Trucks, H. B. Schlegel, G. E. Scuseria, M. A. Robb, J. R. Cheeseman, J. A. Montgomery, Jr., T. Vreven, K. N. Kudin, J. C. Burant, J. M. Millam, S. S. Iyengar, J. Tomasi, V. Barone, B. Mennucci, M. Cossi, G. Scalmani, N. Rega, G. A. Petersson, H. Nakatsuji, M. Hada, M. Ehara, K. Toyota, R. Fukuda, J. Hasegawa, M. Ishida, T. Nakajima, Y. Honda, O. Kitao, H. Nakai, M. Klene, X. Li, J. E. Knox, H. P. Hratchian, J. B. Cross, V. Bakken, C. Adamo, J. Jaramillo, R. Gomperts, R. E. Stratmann, O. Yazyev, A. J. Austin, R. Cammi, C. Pomelli, J. W. Ochterski, P. Y. Ayala, K. Morokuma, G. A. Voth, P. Salvador, J. J. Dannenberg, V. G. Zakrzewski, S. Dapprich, A. D. Daniels, M. C. Strain, O. Farkas, D. K. Malick, A. D. Rabuck, K. Raghavachari, J. B. Foresman, J. V. Ortiz, Q. Cui, A. G. Baboul, S. Clifford, J. Cioslowski, B. B. Stefanov, G. Liu, A. Liashenko, P. Piskorz, I. Komaromi, R. L. Martin, D. J. Fox, T. Keith, M. A. Al-Laham, C. Y. Peng, A. Nanayakkara, M. Challacombe, P. M. W. Gill, B. Johnson, W. Chen, M. W. Wong, C. Gonzalez, J. A. Pople, Gaussian, Inc., Wallingford CT, **2003**.

[6] a) C. Lee, W. Yang, R. Parr, *Phys. Rev. B* **1988**, *37*, 785–789; b) A. Becke, *J. Chem. Phys.* **1993**, *98*, 5648.

[7] P. J. Hay, W. R. Wadt, *J. Chem. Phys.* **1985**, *82*, 270.

[8] a) K. Fukui, *Acc. Chem. Res.* **1981**, *14*, 363–368; b) C. Gonzalez, H. B. Schlegel, *J. Phys. Chem.* **1990**, *94*, 5523.

[9] V. Barone, M. Cossi, *J. Phys. Chem. A* **1998**, *102*, 1995.

[10] NBO Version 3.1, E. D. Glendening, A. E. Reed, J. E. Carpenter, F. Weinhold, for original literature, see: a) A. E. Reed, F. Weinhold, *J. Chem. Phys.* **1983**, *78*, 4066; b) A. E. Reed, L. A. Curtiss, F. Weinhold, *Chem. Rev.* **1988**, *88*, 899.

[11] NBO is generating an incorrect table for the number of valence orbitals of each angular momentum type. It assumes that the last electron occupies an f orbital but it is actually a d electron and so the LANL2DZ basis does not include f functions.

[12] a) J. S. Prasad, L. S. Liebeskind, *Tetrahedron Lett.* **1988**, *29*, 4257. For studies on Pd^{II}-catalyzed coupling-cyclization of α- or β-amino allenes with allylic halides, see: b) S. Ma, W. Gao, *Tetrahedron Lett.* **2000**, *41*, 8933; c) S. Ma, F. Yu, W. Gao, *J. Org. Chem.* **2003**, *68*, 5943; d) S. Ma, F. Yu, J. Li, W. Gao, *Chem. Eur. J.* **2007**, *13*, 247.

[13] a) A. Michalak, T. Ziegler, *Organometallics* **1999**, *18*, 3998; b) R. J. Deeth, A. Smith, J. Brown, *J. Am. Chem. Soc.* **2004**, *126*, 7144.

[14] In addition to these perpendicular conformations, four parallel structures with the C=C parallel to the σ-Pd–C bond could also be envisioned. However, in these cases the local minima either do not exist at all or are so shallow that the geometry optimizations eventually lead to the perpendicular complexes.

[15] The regioselectivity found here is quite similar to those found in the insertion reactions of alkenes with many neutral Pd^{II} complexes. a) A. Michalak, T. Ziegler, *Organometallics* **2000**, *19*, 1850; b) W. Cabri, I. Candiani, *Acc. Chem. Res.* **1995**, *28*, 2. It can readily be explained by a polarization of the π orbital in alkene toward the CH_2 group.

[16] a) P. J. Harrington, L. S. Hegedus, K. F. McDaniel, *J. Am. Chem. Soc.* **1987**, *109*, 4335; b) J. W. Francis, P. M. Henry, *Organometallics* **1991**, *10*, 3498; c) M. Kimura, Y. Horino, R. Mukai, S. Tanaka, Y. Tamaru, *J. Am. Chem. Soc.* **2001**, *123*, 10401; d) F. Ozawa, H. Okamoto, S. Kawagishi, S. Yamamoto, T. Minami, M. Yoshifuji, *J. Am. Chem. Soc.* **2002**, *124*, 10968; e) K. Manabe, S. Kobayashi, *Org. Lett.* **2003**, *5*, 3241; f) G. W. Kabalka, G. Dong, B. Venkataiah, *Org. Lett.* **2003**, *5*, 893; g) M. Yoshida, T. Gotou, M. Ihara, *Chem. Commun.* **2004**, 1124; h) G. Liu, X. Lu, *Org. Lett.* **2001**, *3*, 3879.

[17] For the stereoselectivity of β-heteroatom elimination, see: a) C. G. Frost, J. Howarth, J. M. J. Williams, *Tetrahedron: Asymmetry* **1990**,

23, 201; b) G. Zhu, X. Lu, *Organometallics* **1995**, *14*, 4899; c) B. Alcaide, P. Almendros, T. Martínez del Campo, *Angew. Chem.* **2006**, *118*, 4613; *Angew. Chem. Int. Ed.* **2006**, *45*, 4501.
[18] X. Lu, G. Zhu, Z. Wang, *Synlett* **1998**, 115, and references therein.
[19] Z. Zhang, X. Lu, Z. Xu, Q. Zhang, X. Han, *Organometallics* **2001**, *20*, 3724.
[20] For a computational study, see: D. Balcells, F. Maseras, B. A. Keay, T. Ziegler, *Organometallics* **2004**, *23*, 2784.
[21] S. Hong, T. J. Marks, *Acc. Chem. Res.* **2004**, *37*, 673.
[22] For the sole report on lanthanide-catalyzed hydroalkoxylations of allenols, see: X. Yu, S. Seo, T. J. Marks, *J. Am. Chem. Soc.* **2007**, *129*, 7244.
[23] S. Tobisch, *Chem. Eur. J.* **2007**, *13*, 9127.
[24] S. Tobisch, *J. Am. Chem. Soc.* **2005**, *127*, 11979.
[25] a) S. Tobisch, *Chem. Eur. J.* **2006**, *12*, 2520; b) for a computational mechanistic study of the organolanthanide-mediated intermolecular hydroamination of 1,3-dienes and primary amines, see: S. Tobisch, *Chem. Eur. J.* **2005**, *11*, 6372.

Received: October 2, 2008
Published online: January 8, 2009

